

THE \hat{G} INFRARED SEARCH FOR EXTRATERRESTRIAL CIVILIZATIONS WITH LARGE ENERGY SUPPLIES. III. THE REDDEST EXTENDED SOURCES IN *WISE*

ROGER L. GRIFFITH^{1,2}, JASON T. WRIGHT^{1,2}, JESSICA MALDONADO³, MATTHEW S. POVICH³, STEINN SIGURDSSON^{1,2},
BRENDAN MULLAN⁴

Draft version March 7, 2025

ABSTRACT

Nearby Type III (galaxy-spanning) Kardashev supercivilizations would have high mid-infrared (MIR) luminosities. We have used the Wide-field Infrared Survey Explorer (*WISE*) to survey $\sim 1 \times 10^5$ galaxies for extreme MIR emission, 10^3 times more galaxies than the only previous such search. We have calibrated the *WISE* All-sky Catalog pipeline products to improve its photometry for extended sources. We present 563 extended sources with $|b| \geq 10$ and red MIR colors, having visually vetted them to remove artifacts. No galaxies in our sample host an alien civilization reprocessing more than 85% of its starlight into the MIR, and only 50 galaxies, including Arp 220, have MIR luminosities consistent with $> 50\%$ reprocessing. Ninety of these (likely) extragalactic sources have little literature presence; in most cases they are likely barely resolved galaxies or pairs of galaxies undergoing large amounts of star formation. Five are new to science and deserve further study. The Be star 48 Librae sits within a MIR nebula, and we suggest that it may be creating dust. *WISE*, 2MASS, and *Spitzer* imagery shows that IRAS 04287+6444 is consistent with a previously unnoticed, heavily extinguished cluster of young stellar objects. We identify five “passive” (i.e. red) spiral galaxies with unusually high MIR and low NUV luminosity. We search a set of optically “dark” H I galaxies for MIR emission, and find none. These 90 poorly understood sources and five anomalous passive spirals deserve follow-up via both SETI and conventional astrophysics.

Subject headings: extraterrestrial intelligence – infrared: galaxies

1. INTRODUCTION

This is the third paper in a series describing the \hat{G} infrared search for extraterrestrial civilizations with large energy supplies. The first two papers (Wright et al. 2014b,a) provide the justification and framework for the search. Here we give a brief summary of those works, and the purpose of this paper.

1.1. Justification

Hart (1975) argued that the failure of SETI to date was because humanity is alone in the Milky Way, based on a comparison of likely colonization timescales for the Milky Way and its age. Hart’s argument also implies that any galaxy with a spacefaring species will become thoroughly colonized in a time short compared to the galaxy’s age, suggesting that most galaxies should either contain no spacefaring species or be filled with them.

Kardashev (1964) parameterized potential alien civilizations by their energy supply compared to the starlight available to it, with a Type I civilizations (K1 in our notation) commanding its planet’s entire stellar insola-

tion, a Type II civilization commanding an entire star’s luminosity (i.e. a Dyson sphere, K2), and a Type III civilization (K3) commanding most of the stellar luminosity in a galaxy. Expressed in these terms, Hart’s argument is that the timescale for the appearance of the first K2 to its growth into a K3 is very short, implying that we should expect many K3 civilizations in the Universe if spacefaring life is common.

Indeed, the technological sophistication required to construct a Dyson sphere seems far greater than that required for achieving interstellar travel: while humanity’s solar panels currently fall short of complete coverage of the Sun by a factor of $\sim 10^{17}$, our deepest space probes today these fall short of the distance to the nearest star by a factor of only a few thousand.

If Hart’s reasoning is sound, then we should expect that, unless intelligent, spacefaring life is unique to Earth *in the local universe*, other galaxies should have galaxy-spanning supercivilizations, and a search for K3’s may be fruitful. If there is a flaw in it, then intelligent, spacefaring life may be endemic to the Milky Way in the form of many K2’s, in which case a search within the Milky Way would be more likely to succeed. It is prudent, therefore, to pursue both routes.

1.2. Prior Searches and the Promise of *WISE*

Dyson (1960) and Slysh (1985) demonstrated that waste heat would be an inevitable signature of extraterrestrial civilization, and that such signatures might be detectable to mid-infrared (MIR) instrumentation for civilizations with energy supplies comparable to the lu-

¹ Department of Astronomy & Astrophysics, 525 Davey Lab, The Pennsylvania State University, University Park, PA, 16802, USA

² Center for Exoplanets and Habitable Worlds, 525 Davey Lab, The Pennsylvania State University, University Park, PA 16802, USA

³ Department of Physics and Astronomy, California State Polytechnic University, Pomona, 3801 West Temple Ave, Pomona, CA 91768, USA

⁴ Carnegie Science Center, 1 Allegheny Ave. Pittsburgh, PA 15212, USA

minosity of their host star. The first effective all-sky search sensitive to such namesake “Dyson spheres” was performed by *IRAS*, but the infrared cirrus and the poor angular resolution of *IRAS* limited its sensitivity to only the brightest sources.

Carrigan (2009a) and Carrigan (2009b) used the *IRAS* low resolution spectrometer (LRS) to determine whether candidate Dyson spheres’ SEDs were consistent with blackbodies with $T = 100\text{--}600\text{K}$. Carrigan concluded from infrared colors and low resolution spectra that the best of these of the most Dyson sphere candidates were typically reddened and dusty objects such as heavily extinguished stars, protostars, Mira variables, AGB stars, and planetary nebulae (PNs). Nonetheless, of the 11,000 sources he studied, Carrigan identified a few weak Dyson sphere candidates with spectra consistent with carbon stars. One candidate, IRAS 20369+5131, showed a nearly featureless blackbody spectrum with $T = 376\text{K}$, but Carrigan concluded it is likely a distant red giant with no detectable SiC emission.

Jugaku & Nishimura performed a series of follow-up searches of sources with anomalously red ($K-12\mu$) colors (Jugaku & Nishimura 1991, pp. 295–298; Jugaku et al. 1995; Jugaku & Nishimura 1997, 2000), and found no highly complete Dyson spheres around any of the 365 solar-type stars within 25 pc studied, or another 180 stars within the same distance (Jugaku & Nishimura 2004).

To date, the only search for the waste heat of a K3 civilizations in the peer-reviewed literature has been that of Annis (1999), who searched for outliers to the Tully-Fischer relation to identify K3s intercepting a significant fraction of their starlight. Carrigan (2012) also suggested searching for the morphological signatures of K3s, especially in elliptical galaxies.

The advent of large solid angle, sensitive MIR surveys makes a waste-heat based K3 search more feasible today. The *Wide-field Infrared Survey Explorer* (*WISE*, Wright et al. 2010) performed an all-sky MIR survey at 3.4, 4.62, 12 and 22 μ (the *W1*, *W2*, *W3*, and *W4* bands) with superior angular resolution (by a factor of 5) and sensitivity (by a factor of 1000) than *IRAS*. *WISE* is thus the first sensitive survey for both K2’s in the Milky Way and K3’s among the approximately 1×10^5 galaxies it resolved. The *Spitzer Space Telescope* is another powerful tool for waste heat searches, having superior sensitivity and angular resolution. Its survey of the Galactic plane will be a powerful tool in the search for K2’s in the Milky Way. Since its large area surveys are generally restricted to star-forming regions and the Galactic Plane, where sensitivity to K3’s is more limited, we have restricted our efforts in this paper to *WISE*.

1.3. The AGENT Formalism

In Wright et al. (2014a), we developed the AGENT formalism for quantifying the expected MIR spectra from galaxies hosting K3s in terms of the energy supply of an alien civilization, and outlined the methodology of the *Glimpsing Heat from Alien Technology* (\hat{G}) search for such civilizations in the local Universe using the results of the *WISE* All-sky MIR survey. In particular, we argued in that work that extended sources have the lowest false

positive rate because many of the confounding sources, primarily dusty and extinguished stars and cosmological sources, would not be present in that sample.

The AGENT formalism parameterizes the power used by an alien civilization in terms of starlight absorbed (represented by the parameter α), energy generated by other means (ϵ), thermal waste heat emitted (γ), and other energy disposal (ν).

Most relevant to the present paper are the parameters γ (waste heat luminosity, expressed as a fraction of the starlight available to the civilization) and T_{waste} , the characteristic temperature of the waste heat (which dictates its infrared colors). For values of T_{waste} in the 100–600 K range, values of γ near 1 would imply that most of the luminosity of a galaxy is in the MIR (in the form of the waste heat from alien engines), while values near 0 would imply that the alien waste heat was very small compared to the output of the stars in the galaxy. For dust-free elliptical galaxies with little of their luminosity in the MIR, values of γ of a few percent would be detectable as an anomalous MIR excess.

1.4. Scope and Purpose of this Paper

As an essential step in our waste heat search, we have produced a clean catalog of the reddest sources resolved by *WISE*. The purpose of our focus, in this work, on resolved sources is twofold: resolved sources present their own challenges of interpretation and photometry, necessitating this separate effort; and we wish to first deal with a relatively small and clean sample of nearby galaxies, consistent with a search for nearby K3’s. *WISE* resolves approximately 1×10^5 galaxies (see Section 7.2).

Sources unresolved by *WISE* include a wide variety of potential false positives, such as false detections, data artifacts, cosmologically redshifted objects, dusty objects at cosmological distances, dusty stars, and heavily extinguished stars. The study of these sources requires a different sorts of analysis from those needed for nearby galaxies, which we will describe in later papers. By contrast, there are many fewer, and more easily excluded, sources of false positives among the extended sources in the all sky catalog.

Our primary objective in this paper is to “map the landscape” among galaxies resolved by *WISE* by identifying the nature of the very reddest of these extended sources in the *WISE* All-sky survey, using several metrics for “red-ness”, including the AGENT parameter γ . A byproduct of this effort is a clean catalog of the reddest extended sources in *WISE*, which we present here.

Our secondary objective is to identify and explain the most extreme objects in this catalog, which by their superlative nature are inherently scientifically interesting, regardless of the origin of their MIR luminosity. In most cases, these are well-known objects; in many of the remaining cases their nature seems clear. A few cases, however, are new to the scientific literature and their nature is uncertain. These sources of uncertain nature will be natural candidates for followup, and those that appear consistent with Kardashev civilizations warrant followup by communication SETI efforts, in particular.

As a tertiary objective, we place a zeroth-order upper limit on the energy supplies of nearby K3s by identify-

ing the most MIR-luminous galaxies in our sample. This upper limit can be pushed down to the degree that these galaxies’ MIR emission can be shown have purely natural origins. A rigorous upper limit will require a more detailed analysis of these galaxies’ SEDs, and a more precise calculation of the number of galaxies considered in our sample. We save this exercise for another paper in this series.

Finally, we also illustrate the waste heat approach by performing a quick check of two classes of anomalous galaxies to confirm that they are not hosts to MIR-bright K3’s.

1.5. Plan

In Section 2 we describe how we have analyzed the *WISE* All-sky catalog, and how we performed a series of cuts to select a sample of only real, red, extended sources (our “Extended Gold Sample” of 30,808 sources). Section 2.6 describes how we calibrated the *WISE* photometry, and our estimates of our photometric precision.

Section 3 describes our efforts to classify the sources in the Extended Gold Sample, mostly via SIMBAD object types, so that we could identify previously unstudied sources and reject many Galactic sources.

Section 4 describes our more detailed efforts to understand the reddest sources in the Extended Gold Sample using careful visual inspection and literature searches.

Section 5 describes how we performed a second round of vetting on the Extended Gold Sample, using our calibrated photometry from Section 2.6, our classifications from Section 3, and our visual inspections and literature searches from Section 4 to confidently and carefully identify the reddest sources and determine the best photometry for them on a case-by-case basis. The result is the 563 source “Platinum Sample,” which we present in our catalog, and whose fields are described in Table 4.

Section 6 describes the reddest objects in the Platinum Sample, for several definitions of “red”: all six combinations of the *WISE* bandpasses and the AGENT parameter γ . Section 6.3 describes five sources that are effectively new to science, having little or no literature presence (beyond having been detected with *IRAS*).

We present our conclusions in Section 8, and in the appendices we use the *WISE* imagery to examine two categories of anomalous galaxies, H I dark galaxies and so-called “passive spirals,” and show that they do not exhibit sufficient MIR emission to have their anomalous natures explained by the presence of a K3.

2. SAMPLE SELECTION

The *WISE* mission began scientific operations on 2010 January 7 at wavelengths of 3.4, 4.6, 12, and 22 μm , hereafter referred to as *W1*, *W2*, *W3*, and *W4*, respectively. The All-sky Data Release was subsequently issued on 2012 March 14 and reached 5σ point source sensitivities in unconfused regions to better than 0.08, 0.11, 1 and 6 mJy, respectively (Wright et al. 2010). It should be noted that a more recent data release by the *WISE* collaboration, dubbed ALLWISE⁵ was issued on 2013 November

13. The added sensitivity and depth, proper motion measurements and improved flux variability information in the ALLWISE data products means that they supersede the earlier All-sky Data Release Catalog and Atlas for *most* uses. The *WISE* team suggests that the All-sky Release Catalog may have better photometric information for objects brighter than saturation limits in *W1* and *W2* ($W1 < 8.1$ mag and $W2 < 6.7$ mag). Given that our project was well underway before the ALLWISE data release was issued, and the fact that ALLWISE does not add many ($< 1\%$) new, bright and extended sources in *W3*, we rely on the All-sky Data Release measurements for this analysis.

2.1. $12\mu\text{m}$ Extended Sample

The following methodology was used to select the full sample of $12\mu\text{m}$ -selected sources with extended photometric profiles from the *WISE* All-sky catalog. The instrumental profile-fit reduced χ^2_{ν} (W3RCHI2)⁶ was used to distinguish sources with extended profiles (W3RCHI2 ≥ 3) from sources with point source profiles (W3RCHI2 < 3). Given that the majority of sources in the *WISE* All-sky catalog are unresolved in *W3*, i.e. angular sizes $< 6.5''$, we adopt a conservative χ^2_{ν} threshold of 3, which excludes only a small number of marginally resolved sources while admitting a large but manageable number of point sources with anomalously poor point-spread function (PSF) fits. We also required that the uncertainty in the *W3* “standard” aperture magnitude to be measured (i.e. not null). A null result means that the *W3* “standard” aperture magnitude is a limit, or that no aperture measurement was possible. Finally, we applied a cut in the Galactic latitude ($|b| \geq 10$) to remove contamination from nebular emission in the Galactic Plane:

$$W3RCHI2 \geq 3 \text{ and } |b| \geq 10 \text{ and } W3SIGM \text{ is not null}$$

These search criteria yield a total of 202,851 sources, which composes our parent sample.

2.2. Photometry

The *WISE* All-sky database provides photometry measurements using a variety of methods: PSF profile fitting, variable aperture photometry (eight circular apertures), curve of growth (COG) aperture photometry, and elliptical aperture photometry (for sources matched to the 2MASS Extended Source Catalog (XSC)).

The profile fitting photometry is referred to as W#MPRO and is defined as the magnitude measured with profile-fitting photometry. In addition to magnitudes this procedure also derives the signal-to-noise ratio (SNR) and WRCHI2 (i.e., the goodness of fit to the PSF model of the source) or the goodness of fit to a PSF model of the source.

The COG or “standard” aperture photometry is referred to as W#MAG. According to the *WISE* explanatory supplement “This is the curve-of-growth corrected source brightness measured within an $8.25''$ radius circular aperture centered on the source position. The back-

⁵ <http://wise2.ipac.caltech.edu/docs/release/allwise/>

⁶ We refer to fields/nomenclature in the All-sky catalog in all caps

ground sky reference level is measured in an annular region with inner radius of $50''$ and outer radius of $70''$ ^{7,8}.

The *WISE* pipeline performed nested circular aperture photometry. They used eight apertures from $5.5''$ to $24.75''$ in W1-W3 and $11''$ to $49.5''$ in W4⁸. They provide these in the form of parameters named W#MAG_1 for the first aperture of $5.5''$ in W1 through W3 and $11''$ in W4, W#MAG_2 for the 2nd aperture, W#MAG_3 for the 3rd aperture and so on.

The elliptical aperture measurements, referred to as W#GMAG were based on matched sources between *WISE* and the 2MASS Extended Source Catalog (XSC). The shape of the elliptical aperture was determined by utilizing the shape information of the source provided by the 2MASS XSC. We discuss the uncertainties in our best photometry from calibrating aperture magnitudes to careful extended source photometry in Section 2.6.

Since our analysis is primarily interested in identifying galaxy-scale extraterrestrial civilizations K3s, we required that photometric measurements of extended sources in *WISE* be as reliable as possible. The PSF profile fitting photometry is best used when extracting photometry from point-like sources in the *WISE* survey. For the majority of extended sources in *WISE*, the COG photometry generally provides more reliable measurements, though the strict $8.25''$ radius circular aperture fails for large and extended galaxies. Measuring reliable photometry for extended galaxies has historically proven to be a non-trivial and difficult task, the reason being that galaxies come in all shapes and sizes, and a single “standard” aperture fails to encompass the full range of galaxy sizes and structures.

Recently, Jarrett et al. (2012) have attempted to extract reliable galaxy photometry for extended sources in the *WISE* catalog. They have developed a complex algorithm in order to construct the *WISE* High Resolution Galaxy Atlas and present their initial results in Jarrett et al. (2013). Even more recently, Tom Jarrett has measured reliable photometry for $\sim 67,000$ extended sources in the *WISE* catalog contained within the South Galactic Cap (SGC: $b < -60$). We use this analysis to calibrate the aperture magnitudes as presented by the *WISE* All-sky database, as we describe in Section 2.6

2.3. Quality Flags

In order to remove spurious sources we use the contamination and confusion flags (CC_FLAG) given for W3. In Figure 1, we describe the definitions and provide the number counts of objects having the various CC_FLAGS. We retain sources with the following CC_FLAG: ‘0’, ‘d’, ‘h’, and ‘o’. We consider sources with CC_FLAG ‘P’, ‘p’, ‘D’, ‘H’ and ‘O’ to be contaminated and we removed them from further analysis. Our decision for choosing these particular flags are motivated on empirical examination of a significant fraction of the flagged entries (i.e. we found that the rejected flags have very good reliability in flagging false sources, but the ones we retain often appear for real sources). Using these

⁸ http://wise2.ipac.caltech.edu/docs/release/allsky/expsup/sec2_2a.html

quality flags reduces the $12\mu\text{m}$ sample to 132,651 sources.

2.4. Coordinate and Color Cuts

In addition to removing the Galactic Plane, we also applied three additional coordinate cuts to remove the most obvious high density regions of foreground contamination from objects in star-forming regions. Region 1 is composed of the Galactic Bulge, (i.e., $-12 < l < 10$ and $20 < b < 10$); the total area covered by this region is 212.23 deg^2 and contained 9,323 sources. We removed all sources in Region 1 from our sample. Region 2 comprises sources associated with the Large Magellanic Cloud (LMC); this region contains a total of 13,104 sources. Region 3 is composed of sources associated with the Orion Nebula and contains a total of 12,733 sources. Instead of imposing a blanket coordinate cut for these regions of patchy contamination, we found that we could rather reliably identify foreground sources by rejecting highly clustered sources and retaining relatively isolated sources using a surface density algorithm. This reduces our sensitivity to K3s in regions 2 and 3 without rendering us completely blind to them. After we removed the sources in these three regions, the $12\mu\text{m}$ sample was reduced to 97,491 sources.

We use two simple color cuts to eliminate the most obvious stellar contaminants (it should be noted that these cuts also eliminate a large number of elliptical galaxies, since these generally tend to be blue in the infrared). We identify the stellar locus in the lower left (blue) corner of the diagram (since stellar photospheres have neutral MIR colors) and use the following criteria

$$W2M\text{PRO} - W3M\text{PRO} < 2 \text{ and } W3M\text{PRO} - W4M\text{PRO} \leq 1$$

to remove them from further analysis. We are motivated to use the profile fit photometry because these sources are considered to be stellar-like and thus should have reliable profile fitting photometry.

We visually examined a representative sample of sources in this region and concluded that they are indeed stellar-like objects with anomalously high W3RCHI2 values and since we are primarily concerned with red extended objects, this cut is compatible with our overall search. These criteria identified a total of 21,645 stellar-like sources, leaving 75,846 sources in the $12\mu\text{m}$ extended sample for further inspection. We present a color-color map of these sources in Figure 3.

2.5. Visual Classification

We constructed $2' \times 2'$ *WISE* color images ($(W1+W2)/2 = \text{Blue}$, $W3 = \text{Green}$, and $W4 = \text{red}$) for the remaining 75,846 sources and have visually classified them into five primary groups. The five groups are: **stellar artifacts**, **low coverage artifacts**, **nebular**, **needs closer inspection**, and **high quality**. Representative examples are presented in Figure 4.

The **stellar artifacts** comprise 11,033 sources which were caused by bright saturated stars (i.e., halos, streaks, and latents). Most of these did not have any CC_FLAGS indicating a problem in the All-sky release.

The **low coverage artifacts** are sources which are likely an artifact because they were observed fewer than

W3 CC flag	N total	
0	= 103847	0 (number zero) - Source is unaffected by known artifacts.
P	= 17614	P,p - Persistence. Source may be a spurious detection of (P) or contaminated by (p) a short-term latent image left by a bright source
p	= 516	
D	= 17789	D,d - Diffraction spike. Source may be a spurious detection of (D) or contaminated by (d) a diffraction spike from a nearby bright star on the same image
d	= 18774	
H	= 11182	H,h - Halo. Source may be a spurious detection of (H) or contaminated by (h) the scattered light halo surrounding a nearby bright source
h	= 9286	
O	= 23099	O,o (letter "o") - Optical ghost. Source may be a spurious detection of (O) or contaminated by (o) an optical ghost image caused by a nearby bright source
o	= 744	

FIG. 1.— Description of cc flags, copied verbatim from the *WISE* supplementary catalog.^a

^aAvailable online at http://wise2.ipac.caltech.edu/docs/release/allsky/expsup/sec2_2a.html#cc_flags

6 times by *WISE* under nominally good conditions (i.e. $W3M < 6$, where $W3M$ gives the number of individual 8.8s $W3$ exposures on which a profile-fit measurement of the source was possible). To put this number in perspective, the median $W3M$ for all 202,851 sources was 13. There were a total of 14,595 low coverage sources. We visually examined this sample and recovered 215 sources, which, though having low coverage, appear to be real astrophysical sources and are considered for further analysis.

The **nebular** sources comprise 12,989 sources and we determined them to be locally bright regions of large, nebular networks of Galactic dust, and so not discrete objects. These sources required images with a much larger FOV ($20' \times 20'$) to be classifiable. Since these are highly extended in nature we first identified sources within a $10'$ radius and constructed $20' \times 20'$ color images. The brightest $W3$ source within a cluster was used as the center of a single color image for the field. We recovered 192 sources that appeared to be ‘nebular’ in the $2' \times 2'$ image, but we reclassified as being discrete objects after inspecting the $20' \times 20'$ images.

There were 4,727 sources lacking a 2MASS association the we labeled **for closer inspection**, since they appear to be legitimate sources with good coverage. The majority of these sources were duplicates of sources already included in the **high quality** sample. The sources

which were unique were rematched to the 2MASS catalog using a two-fold process: The first matching used a $30''$ radius and recovered photometry for 509 sources. The second matching used a $60''$ search radius and recovered photometry for 44 sources.

Figure 5 illustrates the typical colors and magnitudes of these categories of sources, and of the $W3$ Extended Gold Sample (i.e. our sample of *real* sources extended in $W3$ with red MIR colors).

We identified 32,502 sources which had 2MASS associations and appear to be real astrophysical objects based on their color images as **high quality** sources. Some extended objects appear in the catalog multiple times. We removed the duplicate entries (those within $60''$) of the brightest entry in the catalog. We identified a total of 1,694 duplicated sources which we removed from the sample.

The number of galaxies we have in our final sample here makes sense. Most of the high latitude extended sources in *WISE* are galaxies, and as we show in Section 7.2, there are approximately 100,000 galaxies that would be extended in the $W3$ *WISE* band if they had significant $W3$ emission. We have thus selected approximately the reddest 1/3 of the galaxies on the sky larger than the angular resolution of the *WISE* $W3$ band.

We have thus constructed a sample of mostly real, extended, and discrete sources in the *WISE* All-sky release

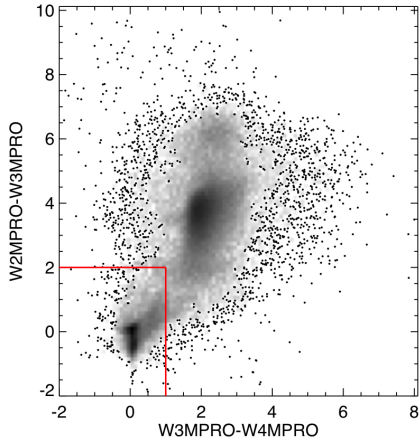


FIG. 2.— W3MPRO - W4MPRO versus W2MPRO - W3MPRO for a sample of $\sim 70,000$ sources. We use this diagram to identify the stellar locus and remove these sources from further analysis.

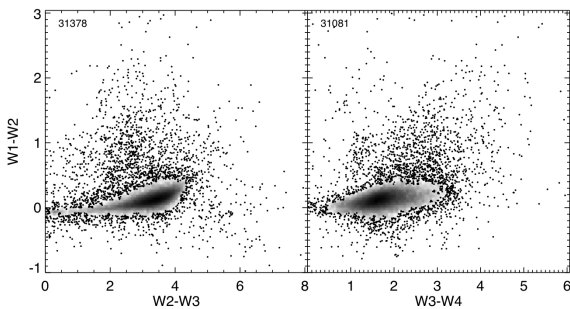


FIG. 3.— Corrected W1CMAG - W2CMAG versus W2CMAG - W3CMAG (*left*) and W3CMAG - W4CMAG (*right*) for the W3 Extended Red Sample (i.e. our sample of All-sky entries that appear to be extended in W3 and with red MIR colors). High density regions are represented in a logarithmic greyscale; the total number of sources in each plot is listed in the plot’s corner.

which we refer to as the *W3 Extended Gold Sample*.

We summarize the vetting procedure that produced the W3 Extended Gold Sample in Figure 6 and present the sky distribution for this sample in Figure 7

2.6. W3 Extended Gold Sample Photometric Calibration

The W3 Extended Gold Sample comprises 30,808 apparently extended sources from the **high quality** sample, 597 sources from the **for closer inspection** sample and 192 sources from the **nebular** sample, bringing the final sample to 31,597 sources (shown in the lower right plot of Figure 5). As discussed in Section 2.5, the *WISE* COG photometry is generally reliable for most sources in this sample, but some care must be taken before using these measurements.

Tom Jarrett has kindly provided us with a preliminary version of his extended source catalog for the south Galactic Cap ($b < -60$) in advance of this catalog’s publication. To further calibrate the extended source photometry and determine the degree of systematic errors in the *WISE* pipeline extraction for extended sources, we have cross-matched 1,907 *WISE* All-sky sources with sources in Jarrett’s preliminary catalog (210 sources did not match, usually because the source was only marginally extended in one of the catalogs). We found that for our W3 Extended Gold Sample, the distribution of differences between the All-sky COG magnitudes and Jarrett’s magnitudes were significantly offset from zero (by 0.4, 0.4, 0.1, and -0.15 magnitudes in W1, W2, W3, and W4) and skewed with long tails past 1 magnitude, with the Jarrett magnitudes typically brighter than the COG magnitudes. In Figure 8 we present the comparison between the COG magnitudes presented in the All-sky release to those measurements presented in Jarrett’s preliminary catalog.

We estimated the size of the sources using the difference between the profile, 4th, and 8th aperture magnitudes, W_{profile} , $W_{\#4}$, and $W_{\#8}$. For unblended point sources these magnitudes are typically identical, but for extended sources the larger aperture magnitudes are more faithful, because they measure flux further up the curve of growth. We formed “size” parameters from the quantities $(W_{\#8} - W_{\#4})$ and $(W_{\#8} - W_{\text{profile}})$, and found that by using the $W_{\#8}$ magnitudes, with quadratic corrections in the size parameters and constant offsets, we could reproduce the Jarrett magnitudes to within 0.06 mag in most cases and colors to within 0.08 mag.

The transformation we used to generate accurate extended source magnitudes $W_{\#}$ from the *WISE* pipeline photometry is:

$$S1 = W_{\#8} - W_{\#4} \quad (1)$$

$$S2 = W_{\#8} - W_{\text{profile}} \quad (2)$$

$$W_{\#} = a_0 + a_8 W_{\#8} + a_{s1,1} S1 + a_{s2,1} \quad (3)$$

$$S2 + a_{s1,2} S1^2 + a_{s2,2} S2^2 \quad (4)$$

We performed a singular value decomposition to determine the best values for the coefficients, and report our coefficients in Table 1:

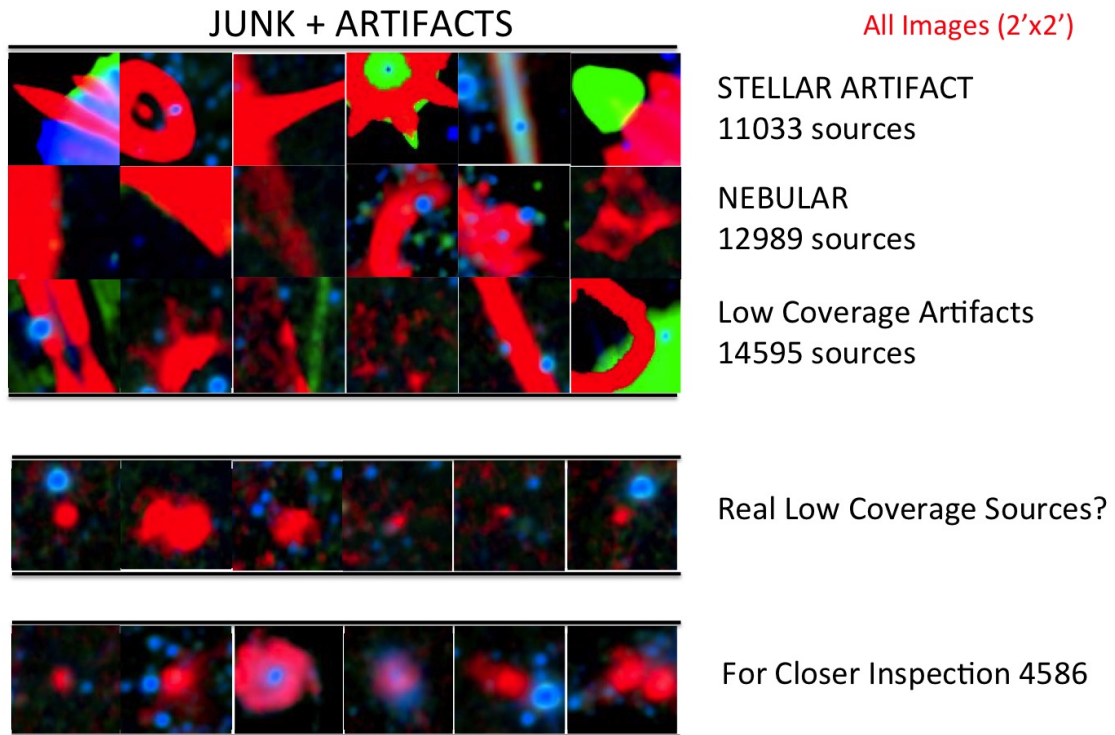


FIG. 4.— We present examples of the color images for the visually classified sources. The top 3 rows show cases where the source is considered to be the most obvious examples of astrophysical and instrumental artifacts. The fourth row shows sources with low coverage $W3M \leq 5$ but which could potentially be real astrophysical sources. The fifth row shows sources with nominal coverage but lacking 2MASS associations. Some such objects are real sources (often blends of multiple sources), and we separated these from artifacts by visual inspection.

TABLE 1
CORRECTION COEFFICIENTS TO PRODUCE CORRECTED
MAGNITUDES FOR EXTENDED SOURCES.

band	a_0	a_8	$a_{s1,1}$	$a_{S2,1}$	$a_{S1,2}$	$a_{S2,2}$
W1	-1.083	1.093	0.107	-0.591	0.021	-1.114
W2	-1.211	1.103	0.246	-1.104	0.062	-1.540
W3	-0.419	1.050	0.030	-0.449	0.049	-1.130
W4	-0.588	1.106	0.006	-1.021	-0.228	0.676

We present a comparison of our corrected photometry to that of the preliminary Jarrett photometry in Figure 9 & 10. Because these distributions are roughly Gaussian but with extended wings, we report the precision of our photometry in three ways. In our figures we show the best-fit Gaussians to each of the residual distributions, and report the width of these Gaussians as σ ; this represents the typical systematic error due to limitations of the *WISE* pipeline for most of our extended sources.

The long wings of the residual distribution typically represent blended and highly structured sources for which our simple calibration scheme failed to match Jarrett’s more careful analysis, and a small number of extreme outliers inflate the standard deviation of these distributions beyond utility. To quantify the systematic photometric errors including the bulk of the non-Gaussian wings in a more robust manner, we calculated a “robust sigma” including outlier rejection⁹, and also the value of the 68th percentile absolute deviation from the median for each magnitude and color combination. We present the results of all three error estimates in Table 2.

While a detailed study of individual targets would benefit from the more precise photometry of Jarrett’s final catalog, this precision is sufficient for the initial exploration of the *WISE* data set and identification of superlative objects.

⁹ Using the IDL routine `ROBUST_SIGMA` written by H. Freudenreich, who cites “Understanding Robust and Exploratory Data Analysis” (Hoaglin et al. 1983)

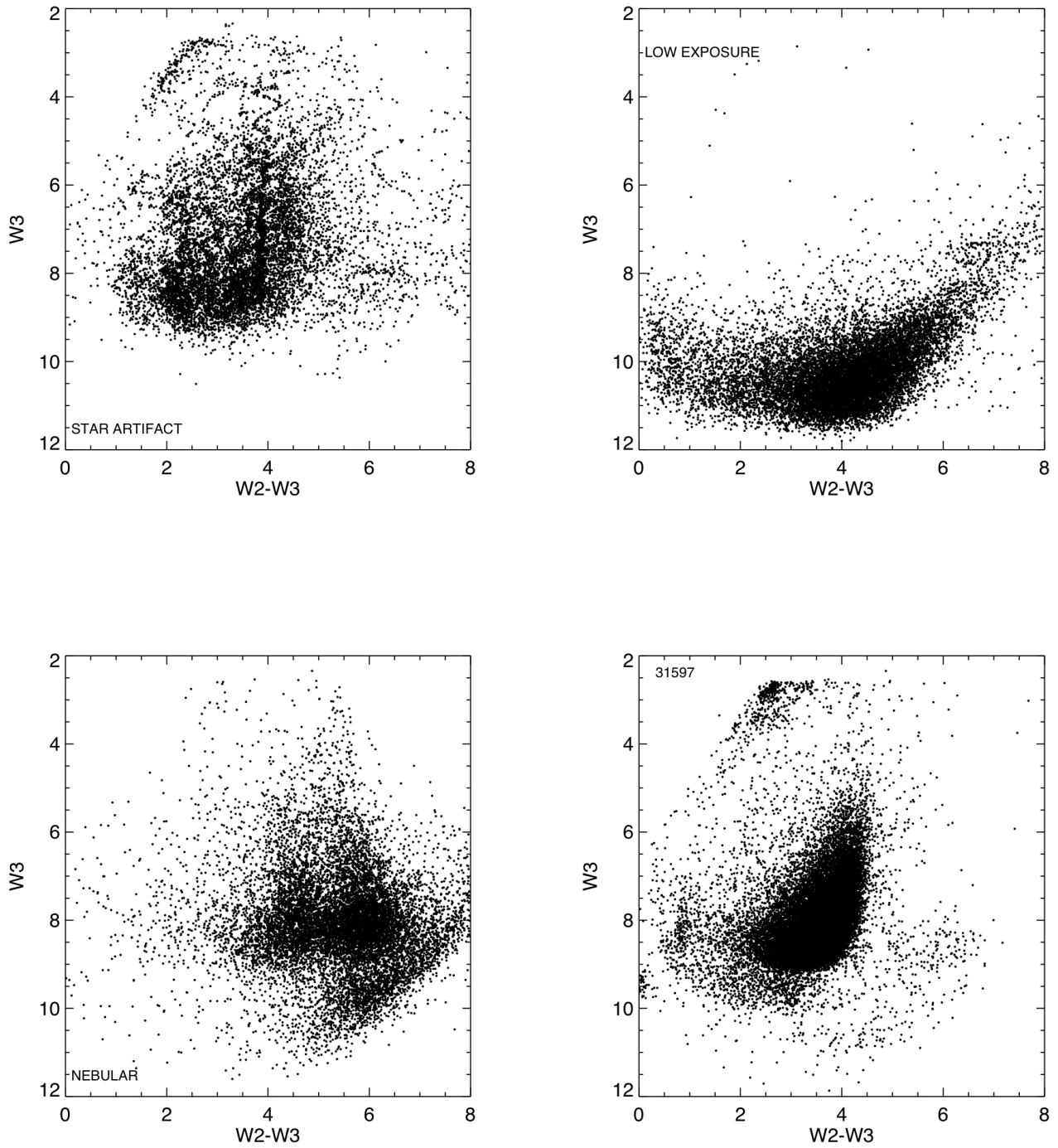


FIG. 5.— We show W3 magnitude versus W2 - W3 color for classified sources. Top Left: Stellar artifacts. Top Right: Low exposure sources. Bottom Left: Nebular type sources. Bottom Right: W3 Extended Gold Sample.

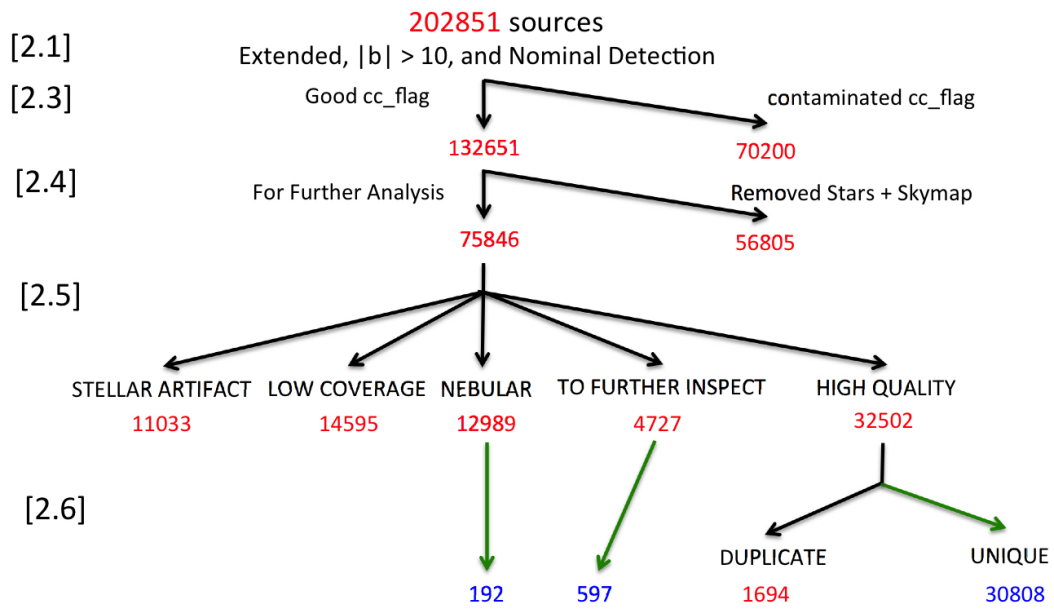


FIG. 6.— Schematic diagram of W3 extended source analysis. Numbers to the left of Figure 6 refer to the section numbers in this manuscript. Extended sources are identified as those with $W3RCHI2 \geq 3$ and nominal detection are those where $W3SIGM$ is not null.

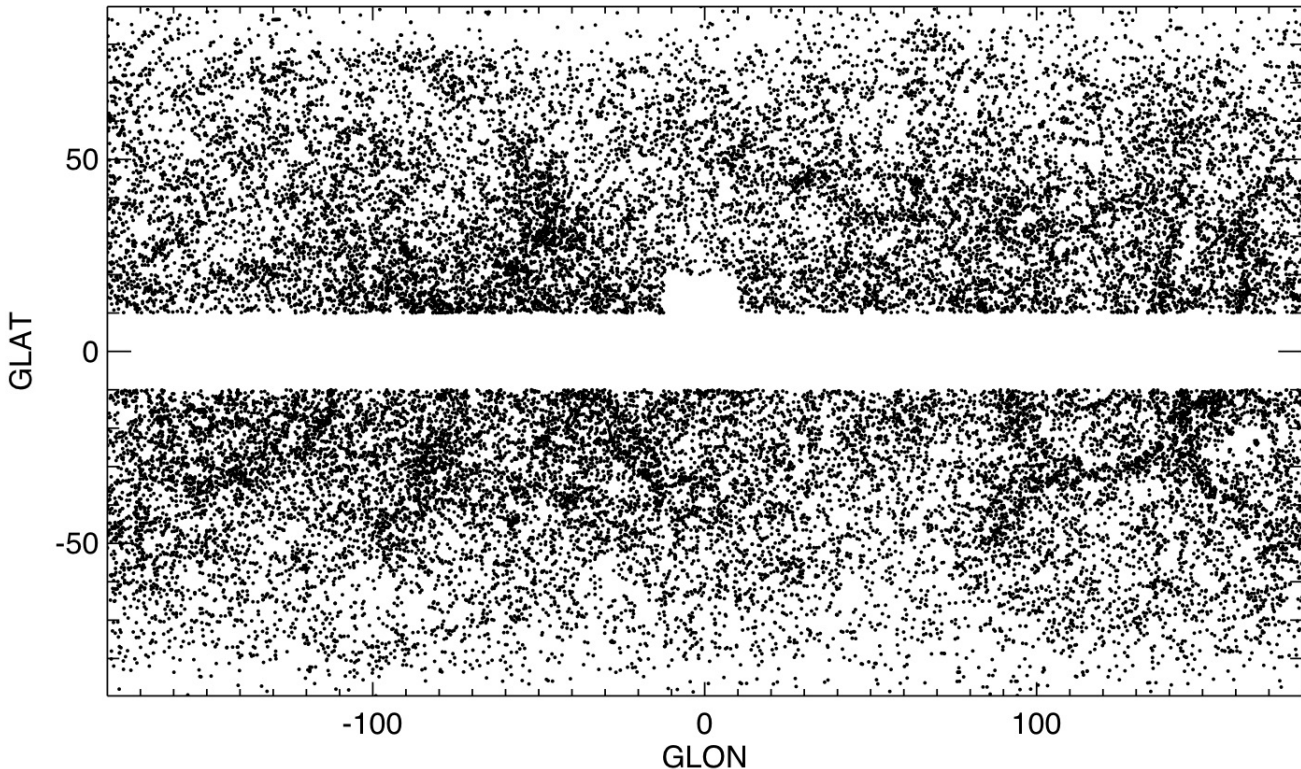


FIG. 7.— We present the sky distribution for the W3 Extended Gold Sample.

TABLE 2
THREE MEASURES OF SYSTEMATIC ERRORS IN OUR
EXTENDED SOURCE PHOTOMETRY.

Quantity	σ	Robust st. dev. (# rejected)	68%-ile
W1	38	54 (148)	54
W2	54	70 (115)	69
W3	39	49 (121)	50
W4	51	81 (142)	84
W1-W2	30	38 (41)	36
W1-W3	42	56 (132)	56
W1-W4	73	100 (132)	100
W2-W3	50	67 (103)	65
W2-W4	79	110 (114)	100
W3-W4	74	100 (73)	90

NOTE. — Values in mmag, measured as the width of the distribution of differences between our calibrated magnitudes and those of a preliminary version of Jarrett’s unpublished extended source photometry. We present three measures: the width of the best-fit Gaussian (σ), the “robust sigma” calculated as a standard deviation with outlier rejection (number of rejected sources in parentheses, out of 1907 total sources), and the 68th percentile absolute deviation from the median. For Gaussian distributions these three quantities should be nearly identical.

3. CHARACTERISTICS OF THE EXTENDED GOLD SAMPLE

To help us characterize sources in the Extended Gold Sample, we employed the source classifications presented in the SIMBAD database, where available, as a starting point. SIMBAD provides over 130 different types of astrophysical classifications ranging from the stellar to the cosmological. We recovered source classifications for $\sim 87\%$ of the Extended Gold Sample. The median distance between the *WISE* and SIMBAD source is of the order $\sim 0''.5$. We find that $\sim 93\%$ of these sources have been categorized as being external galaxies vs. Galactic foreground objects. We find that the 7% that are “stellar” are typically not point sources but are resolved in the IR for some reason. These are encouraging results because they validate our selection and vetting procedures.

In the following sections we discuss the two most commonly identified types of astrophysical sources — those of Galactic origin and those of extragalactic origin, the latter being of primary interest in this study.

3.1. Extragalactic Sources

We have grouped the SIMBAD classifications for extragalactic sources into five broad categories:

- **normal** Galaxy: Includes the following SIMBAD types, Galaxy (G), Galaxy in Pair (GiP), Galaxy in Group (GiG), Galaxy in Cluster (GiC), Cluster of

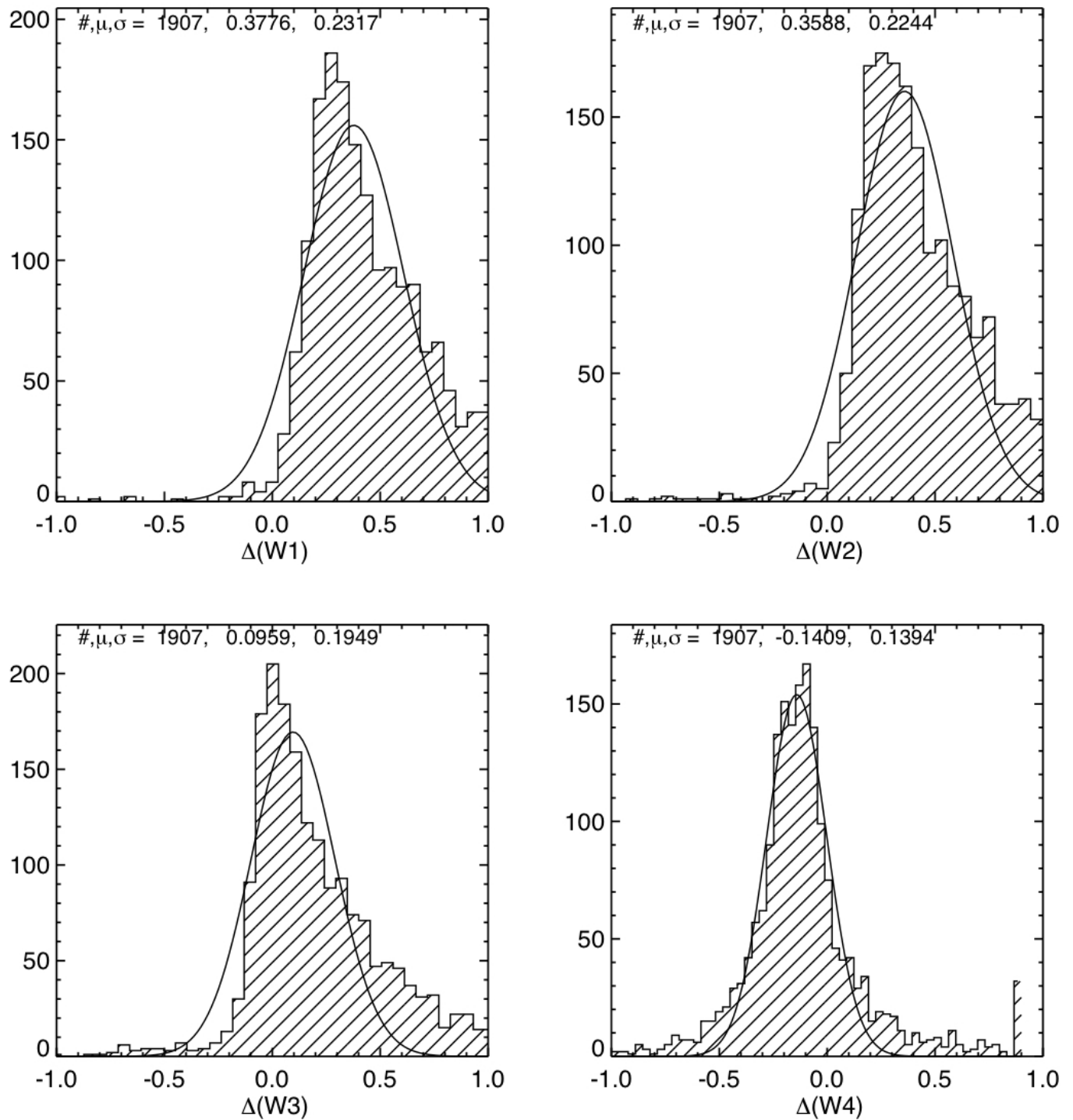


FIG. 8.— *WISE* WMAP (curve-of-growth corrected) All-sky photometry vs. aperture photometry for extended sources in the South Galactic Cap carefully extracted by Tom Jarrett. Numbers in the plots describe the number, mean (μ), and standard deviation (σ) of Gaussian fits to the data. The pipeline photometry has offsets and color-dependent systematic errors for these extended sources.

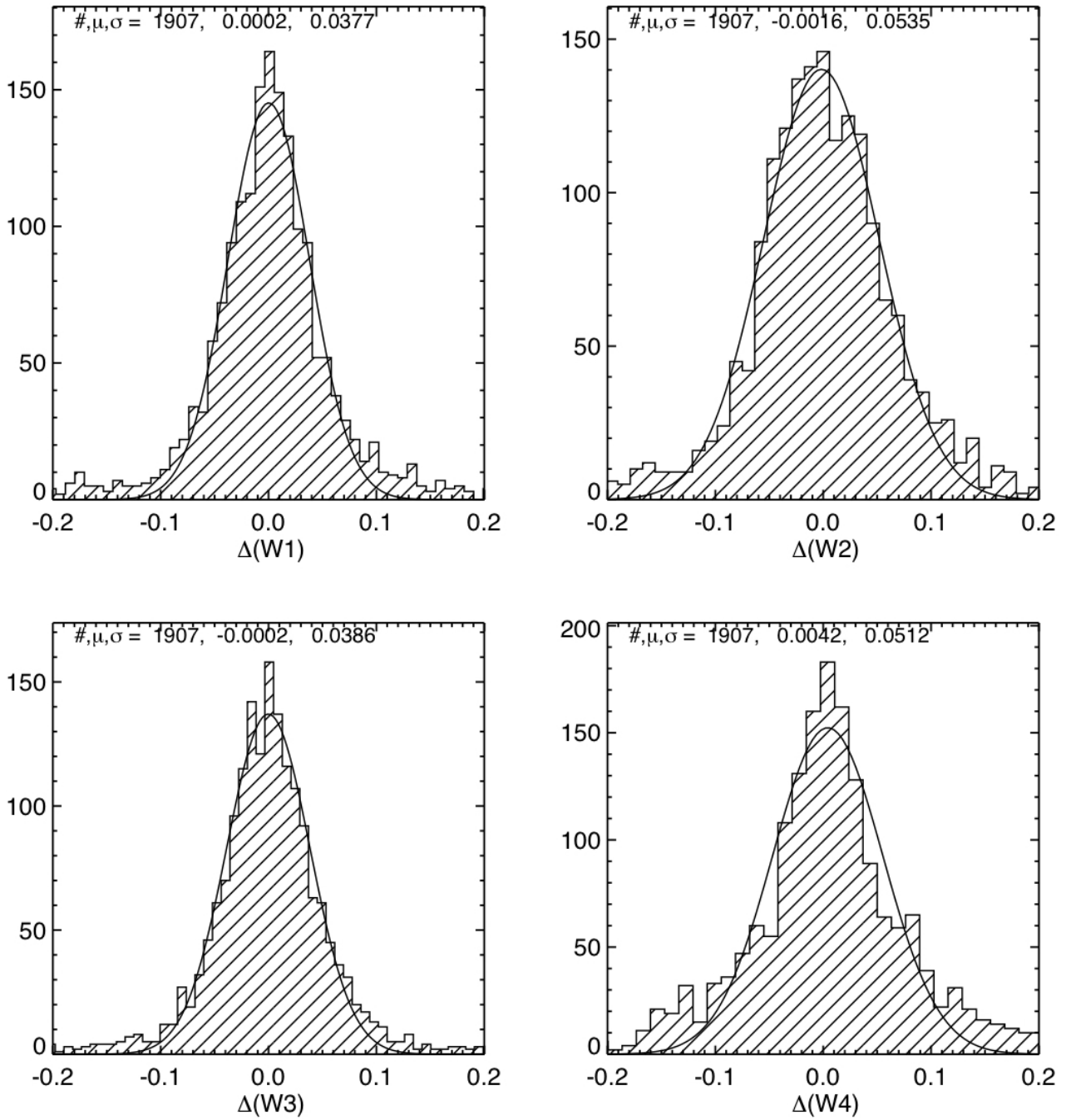


FIG. 9.— Results of our calibration of *WISE* photometry to careful extended source photometry of sources in the south Galactic Cap ($b < -60$) provided by Tom Jarrett. We present the distribution in differences in our corrected *WISE* magnitudes in the four *WISE* bands to the Jarrett photometry for common sources. Numbers in the plots describe the number, mean (μ), and standard deviation (σ) of Gaussian fits to the data. These “corrected” magnitudes have roughly Gaussian errors and little or no systematics with color or size for most sources.

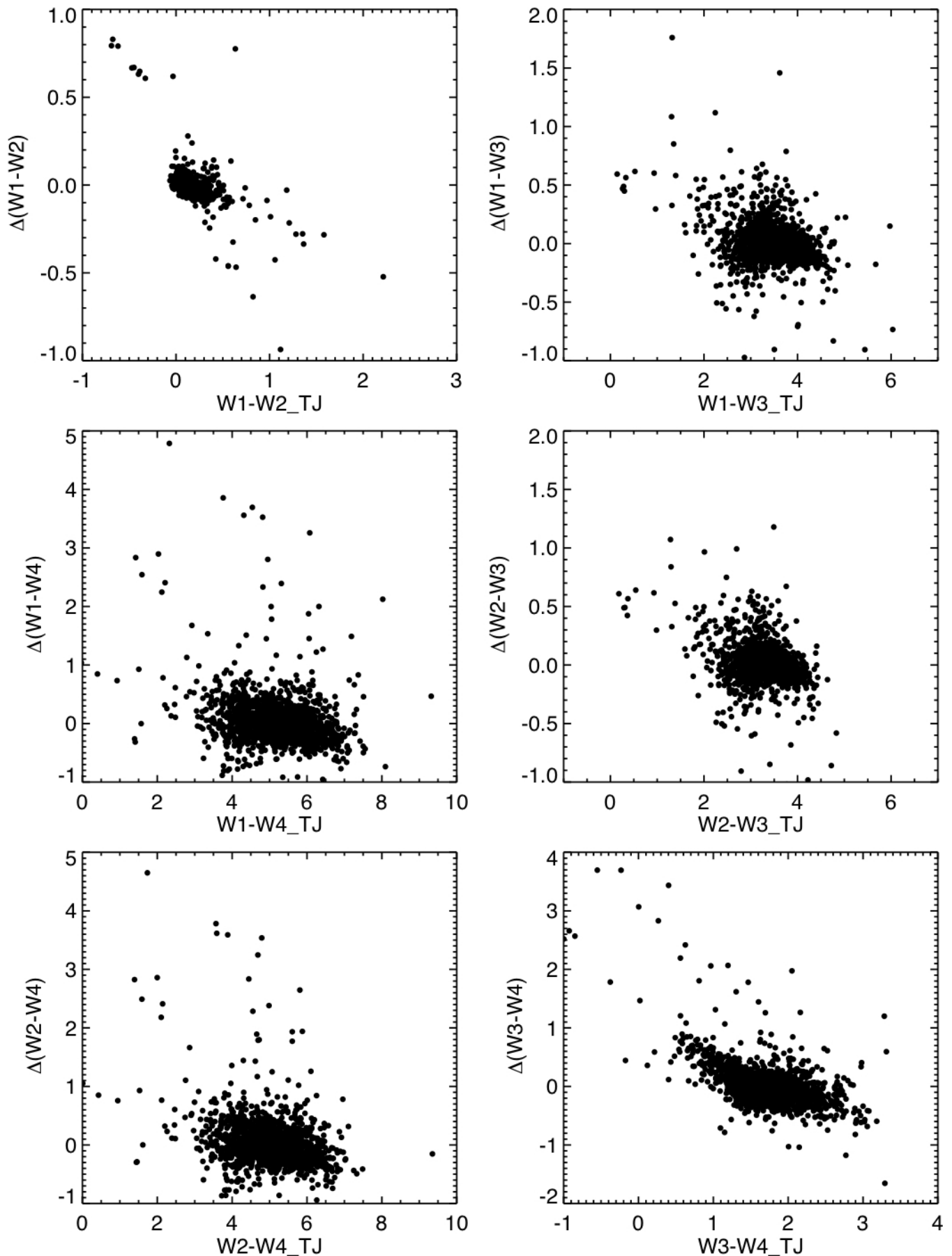


FIG. 10.— Results of our calibration of *WISE* photometry to careful extended source photometry of sources in the south Galactic Cap ($b < -60$) provided by Tom Jarrett. For all six color combinations of the four *WISE* bands (using the Jarrett magnitudes), we present the distribution in differences in our corrected magnitudes to the Jarrett photometry for common sources. Numbers in the plots describe the number, mean (μ), and standard deviation (σ) of Gaussian fits to the data. These “corrected” colors have roughly Gaussian errors and little or no systematics with magnitude or size for most sources.

Galaxies (GlC), Group of Galaxies (GrG), Brightest galaxy in a Cluster (BiC), and Compact Group of Galaxies (CGG)

- **active** Galaxy: LINERS (LIN), QSO, Radio Galaxy (rG), Active Galactic Nuclei (AGN), Seyfert Galaxies (Sy1 + Sy2), BL Lac - type object (BLL), and Blazar (Bla)
- **star-forming** Galaxy: Emission Galaxy (EmG), HII Galaxy (H2G), Starburst Galaxy (SBG), and Blue Compact Galaxy (bcG)
- **interacting** Galaxy: Interacting Galaxy (IG), and Pair of Galaxies (PaG)
- **low surface brightness** Galaxy: low surface brightness galaxy (LSB)

To characterize the galaxy population we construct a simple color-magnitude diagram (W2-W3 versus W3). Figure 11 present W2-W3 versus W3 for a variety of (mostly extragalactic) sources. The two most striking features in this figure are the almost complete absence of galaxies with $W3 > 10.0$, and $W2-W3 \geq 4.5$.

The faint limit is significantly above the *WISE* detection limit in W3 of ~ 11.2 (for point sources), and so requires explanation. This limit originates in our requirement that a galaxy be both detected *and extended* in *WISE* in the W3 band. We measure extended-ness with W3RCHI2, and it appears that this parameter rarely takes values above 3 for sources with $W3 \gtrsim 9$, no matter how extended the object is. This lower limit is thus an artifact of the *WISE* data pipeline and our Extended Gold Sample selection criteria.

The upper left plot shows where the *normal* galaxies and the SIMBAD classification Part of a Galaxy (PoG) reside in this color-magnitude space. These sources compose $\sim 82\%$ of the total galaxy population. In the upper right we show the color-magnitude diagram for star forming and LSB galaxies, which compose $\sim 12\%$ of the population. The lower left shows the active and interacting galaxies, composing $\sim 6\%$ of the population. The lower right plot shows the generic SIMBAD classifications of (IR) and X-ray (X) sources. These last two are somewhat ambiguous classifications, and we include them only for completeness.

These results are quite consistent with our expectations validating the SIMBAD types. The *normal* galaxies appear to occupy the overall parameter space seen in the other populations suggesting this to be a mixture of a variety of galaxy types. The *star-forming* galaxies appear to congregate at redder W2-W3 colors ($W2-W3 \geq 3$), as expected. Interestingly, the LSB galaxies appear to tightly congregate on the fainter end of the *star-forming* population. The *interacting* galaxies appear to populate the same parameter space as seen by the *star-forming* galaxies, which is an expected result as a majority of *interacting* galaxies are experiencing high star formation rates. The *active* galaxies populate similar parameter space as seen in the *normal* galaxy population. The IR sources appear to be a mixture of both extragalactic sources and Galactic sources, though we do see

a tight clustering occupying similar parameter space as the LSB galaxies.

3.2. Galactic Sources

Though *Galactic sources* (i.e. sources within the Milky Way Galaxy) compose only $\sim 7\%$ of our sample it is important to understand how they might produce contamination in our investigation. SIMBAD provides classifications for over 70 different types of these Galactic sources, which we have reduced to six primary types: *normal* stars, Young Stellar Objects (YSO), Variables, Evolved, Evolved + IR, and stars in clusters. Our grouping methodology is as follows:

- **normal** Star: Includes the following types, Star (*), Emission-line Star (Em*), Peculiar Star (Pe*), High proper-motion Star (PM*), Star in double system (*i*), Be Star (Be*), and Eclipsing binary (EB*)
- **YSO**: T Tau-type Star (TT*), Variable Star of FU Ori type (FU*), Herbig-Haro Object (HH), Pre-main sequence Star (pr*), and Young Stellar Object (Y*O)
- **variable** Star: Variable Star (V*), Variable Star of beta Cep type (bC*), Variable Star of Orion Type (Or*), Semi-regular pulsating Star (sr*), Variable Star of W Vir type (WV*), Long-period variable star (LP*), CV DQ Her type (intermediate polar) (DQ*), Variable Star of delta Sct type (dS*), Variable Star of alpha2 CVn type (a2*), Cepheid variable Star (Ce*), Variable Star with rapid variations (RI*), Variable Star of RV Tau type (RV*), Pulsating variable Star (Pu*), Variable Star of Mira Cet type (Mi*), Variable Star of R CrB type (RC*), Eruptive variable Star (Er*), Variable Star of irregular type (Ir*), and Cataclysmic Variable Star (CV*)
- **evolved** Star: Asymptotic Giant Branch Star (He-burning) (AB*), Red Giant Branch star (RG*), Wolf-Rayet Star (WR*), and S Star (S*)
- **evolved+IR** Star: Post-AGB Star (proto-PN) (pA*), Star with envelope of OH/IR type (OH*), and Carbon Star (C*)
- **Star in Cluster**: Star in Cluster (*iC), Cluster of Stars (Cl*), and Star in Nebula (*iN)

For completeness we must also consider two other types of Galactic sources, PN and **Solar System Objects** (SSOs) such as comets, asteroids, and planets. The SSOs are identified by utilizing the *WISE* All-sky Known Solar System Object Possible Association List. We also identify two IR bright planets, Neptune and Uranus, which are included in the sample.

To characterize the *WISE* high latitude Galactic population we present Figure 12, which shows the color-magnitude diagrams for the various Galactic classifications. As before we find that the majority of the Galactic population are relatively rare at $W3 > 10$ and $W2-W3 \geq 4.5$, though we do find sources with very extreme

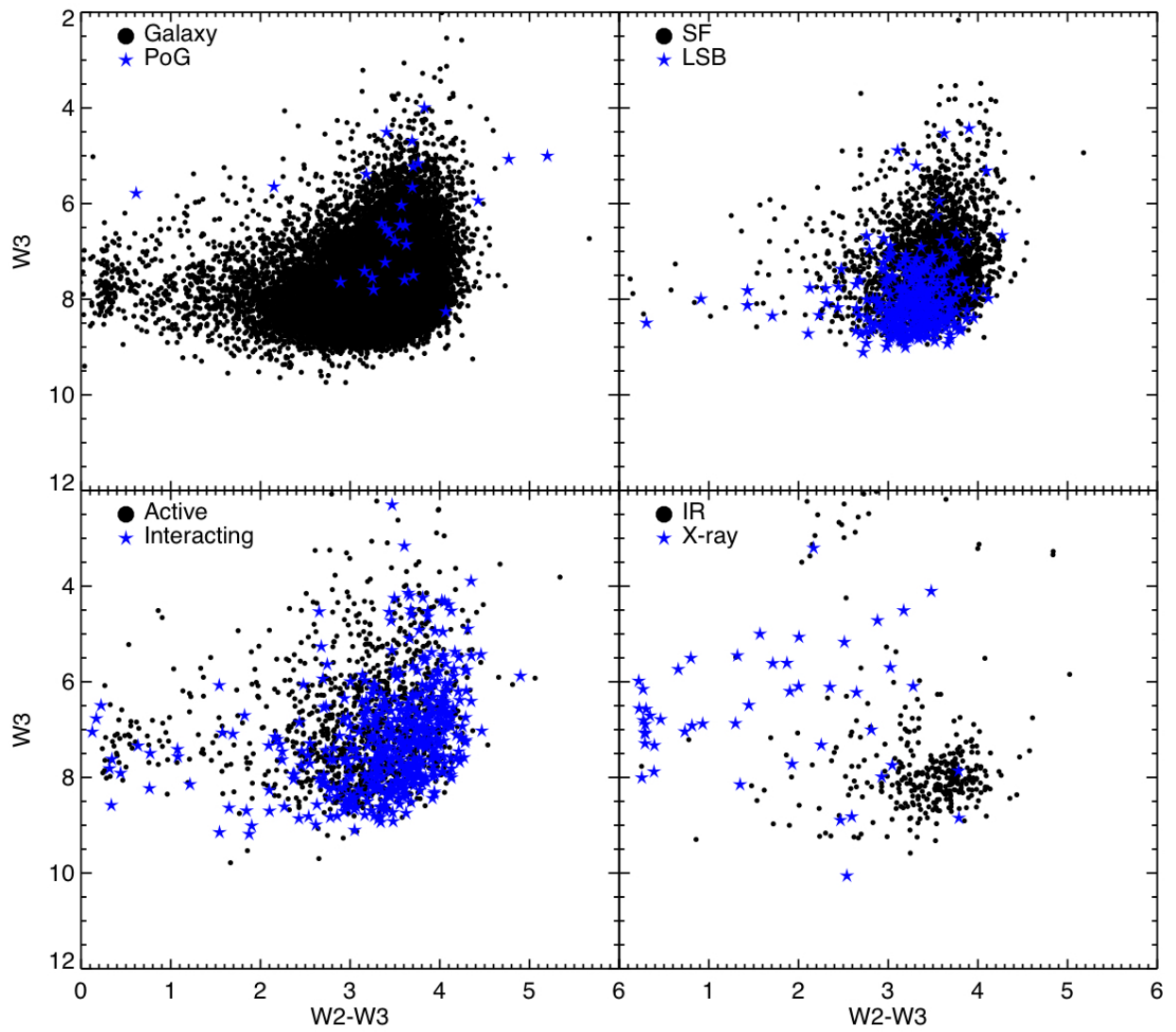


FIG. 11.— Color-magnitude diagrams for a variety of extragalactic sources in the Extended Gold Sample.

W2-W3 colors, i.e. $W2-W3 \geq 6$. We also find, as was expected, that the two types of sources which confuse and contaminate our search the most are the YSO's and planetary nebulae (PNe). While we do find contaminating sources within the Galactic sample, the scarcity of astrophysical sources with $W2-W3 \geq 4.5$ should make our search relatively straightforward for high γ K3's.

4. VISUAL REVIEW AND GRADING OF SOURCES IN THE W3 EXTENDED GOLD SAMPLE

A systematic search into the existence and numbers of possible galaxy-spanning ETIs requires that we carefully inspect the most interesting subsets of the Extended Gold Sample.

4.1. AGENT parameterization

For every source we apply the methodology described in Wright et al. (2014a) to estimate the AGENT parameters γ (the fraction of starlight reradiated as alien waste heat) and T_{waste} (the waste heat's characteristic temperature) for each galaxy, assuming $\nu = 0$ (no nonthermal alien power disposal/emission) and $\alpha = \gamma$ (that is, all of the waste heat originated as stellar power). We fit all four *WISE* bands to the three parameters ($L/4\pi d^2$) (the bolometric flux of the source), γ , and T_{waste} .

For consistency, we modeled every galaxy as having an intrinsic SED represented by the old elliptical SED model *Ell13* of Silva et al. (1998), of which a fraction α of the starlight is absorbed and re-emitted as a blackbody at temperature T_{waste} . Of course, many galaxies have a significant blue stellar population and dust. Because the *Ell13* template has the least MIR emission of all of the Silva et al. (1998) galaxy templates, using it will allow us to measure the *maximum* amount of MIR emission from each galaxy that *could* be attributed to ETI's from *WISE* broadband photometry alone. Its is thus consistent with our desire to set upper limits to K3 waste heat emission.

4.2. Visual inspection

Using γ as the primary parameter for prioritizing sources we inspected, reviewed and graded every source in the W3 Extended Gold Sample with $\gamma \geq 0.25$, ~ 4000 in all.

To facilitate this visual review, we constructed an interactive GUI system. This system provided an “at-a-glance chart” for each source (Figure 13) consisting of $2' \times 2'$ multiwavelength imaging cutouts (DSS, SDSS, 2MASS, and *WISE*) centered on the *WISE* source position, a variety of hyperlinks to supplementary imaging data and database queries centered on the source position (e.g. *WISE* (L1B + Atlas images, SIMBAD, NED), and printed information including source coordinates, *WISE* catalog colors and magnitudes, number of publications listed in SIMBAD, number of times *WISE* observed the source position in each filter (W#M) and number of times *WISE* detected the source in each filter (W#NM).

4.3. Grading and Literature Search

The sample of red, extended objects in *WISE* is a combination of sources, galactic and extragalactic; real and

instrumental; well-studied and new-to-science. We developed a sorting scheme to help us understand it better and prioritize sources for further investigation.

We defined a simple alphabetical grading scheme (A-F):

- A – Astrophysical red source with no previous publications in SIMBAD, little or no ancillary survey data. *Highest priority candidate for observational follow-up.*
- B – Astrophysical red source with some ancillary data or few publications, which do *not* provide convincing evidence that its nature is understood. *Good candidate for follow-up.*
- C – Visual review of source and/or publication list provides convincing evidence that its nature is understood (although in some cases, the SIMBAD classification may be incorrect.)
- D – Astrophysical source that creates artifacts detected as red extended sources by *WISE*. Most frequently associated with a bright star or large region of bright nebulosity.
- F – Fake/false source or artifacts, such as a latent image. *Not* a real astrophysical red source. Does not belong in any astronomical catalog.

We next provide some details of the decision process leading to the assignment of the various grades above, working backwards from F to A.

Grade F. Persistence artifacts, or “latents,” in the W3 band constitute the most common class of false, extended red source meriting an F grade. Most latents are culled by the initial visual classification (see Section 2.5), but some did make it into the Extended Gold Sample. The most pernicious cases involve W3 latents that happen to fall on the positions of legitimate W1+W2 sources; these closely resemble our expectations for a high- γ KIII galaxy in the *WISE* images. The visual review process readily discards such sources. They have very low W3NM/W3M, failing to appear in the majority of the individual *WISE* Level 1b frames (planets, comets, and asteroids also exhibit this behavior, but do so in all bands and appear in the Known Solar System Object Possible Association List, see Section 3.2). The wider-field *WISE* Atlas images typically reveal the bright star responsible for producing a W3 latent.

Grade D. Unlike F-grade sources, sources assigned D grades are real astrophysical objects, but these are not valid, red extended *WISE* sources. There are two main classes: (1) Saturated stars ($W3 \leq 3.8$ mag) which would otherwise be point sources, and (2) bright “knots” within larger regions of mid-IR nebulosity (for example, associated with Galactic foreground emission). Our visual review of the *WISE* images readily identifies such cases.

Grade C. For sources that pass the quality control checks associated with F and D grades above, we next evaluate the citations listed for the associated SIMBAD source(s).

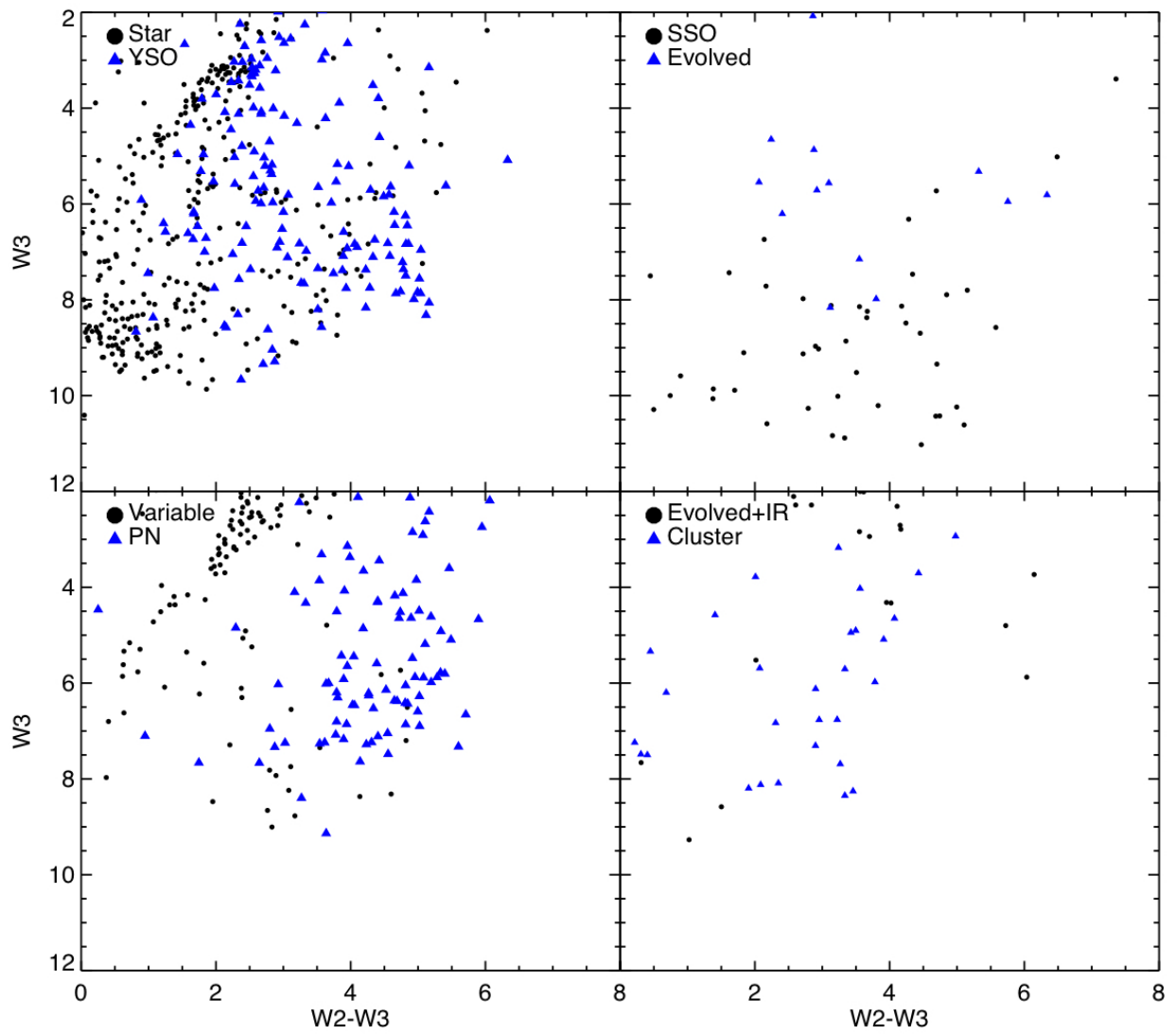


FIG. 12.— Color-magnitude diagrams for a variety of galactic sources in the Extended Gold Sample.

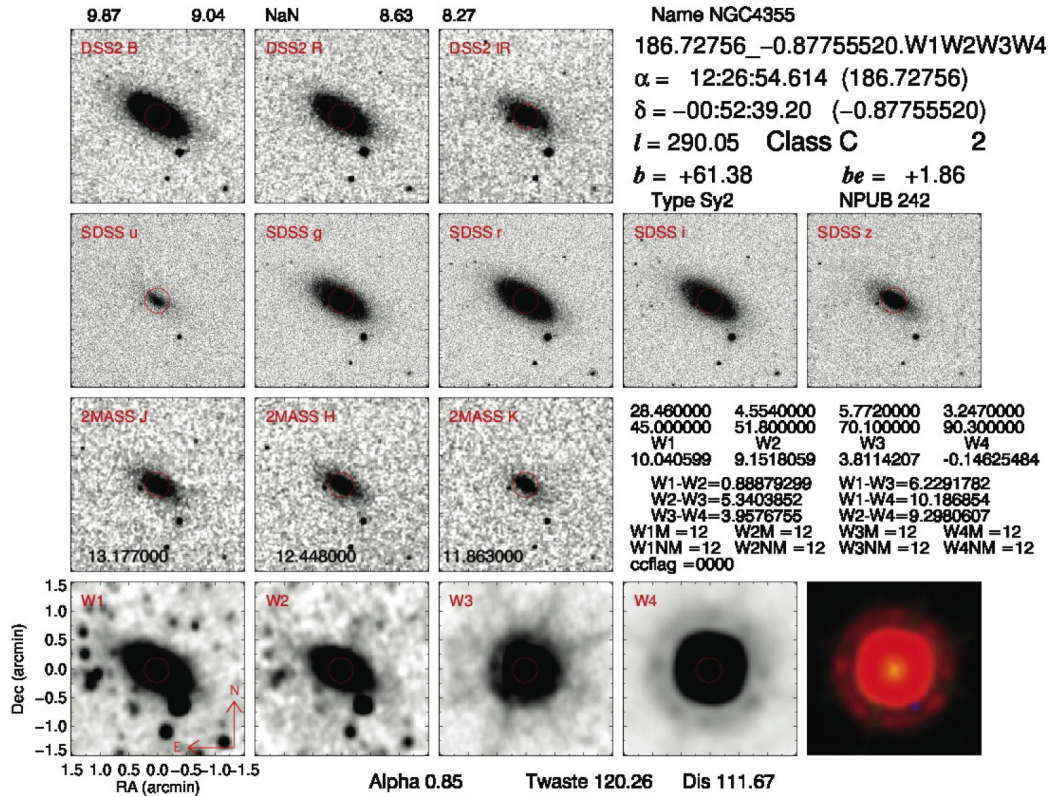


FIG. 13.— Example of an “at-a-glance” chart used for detailed visual review and classification of sources in the Extended Gold Sample. The red labels of the images shows the data sources; the scale is the same in each image and given in the bottom-left-hand image. The magnitudes of the 2MASS imagery are given in the corresponding images. The bottom-right-hand image is a color composite from the four *WISE* bands in the bottom row. The SIMBAD name is in the upper right, along with the file name, J2000 coordinates in sexagesimal and decimal, the galactic coordinates and ecliptic latitude, the SIMBAD type, and the number of publications reported by SIMBAD. “Class” refers to the grade of the source (C in this case, reflecting its large number of associated publications, see Section 4.3). Our *WISE* extended source photometry appears to the right of the third row, including, for each band, the RCHI2 parameter (large values indicate the source is well resolved), the signal-to-noise ratio of the detection, and the magnitude. Also reported are the various color combinations, the number of visits to the field, and the number of visits in which the source was detected. Finally, the contamination and confusion flags (CC.FLAG) are given for the four bands. This particular source, W122654.61-005239.2, illustrates what might pass for a high- γ KIII galaxy in multiwavelength images; it is actually a dusty (and well-studied) Seyfert 2 galaxy.

Sources that receive C grades typically have $\gtrsim 4$ citations, which, taken together, convince us that its astrophysical nature is understood.

If our review of the literature for a given source point toward original object type listed in SIMBAD, we accept that object type. In many cases we found either (1) that the preponderance of literature pointed to a different object type or (2) the nearest SIMBAD source returned by our automated matching was not the appropriate counterpart for the *WISE* source. If necessary, we manually overrode the SIMBAD object type and/or matching source for our catalog.

An example of a grade C source is shown in Figure 13.

Grades B and A. Our final two grades, B and A, represent real astrophysical extended red sources with scant ($\lesssim 4$) or zero existing literature citations, respectively; these sources should be given high priority for further observational followup to determine their nature.

Grade B sources are cited only in large, survey catalogs containing minimal interpretation of individual sources. Commonly encountered catalog papers containing Grade B (and also C) extended red *WISE* sources are listed in Table 3.

The most promising candidates for observational follow-up are grade A sources that are isolated, meaning they are neither part of a cluster of red objects (for example, a young embedded star cluster or a galaxy cluster hosting many mergers) nor associated with diffuse mid-IR nebulosity (a hallmark of embedded star clusters in H II regions or an indication that they may be associated with a large, extended galaxy). An example of an isolated “A” source and a cluster of red sources is presented in Figure 14.

Note that this grading scheme only loosely tracks “interest” from a SETI perspective: a well-studied galaxy might have an anomalously high MIR luminosity and thus be an outstanding SETI target, while a new-to-science protostar might be manifestly ordinary and so very low priority. The “followup” of class A sources is thus primarily to determine their true nature and determine if they warrant further study from either a natural astrophysics or SETI perspective.

Figure 15 illustrates the colors and magnitudes of the sources we have graded, and shows where these sources reside in this parameter space.

5. W3 EXTENDED PLATINUM SAMPLE

5.1. Construction of the Sample

The Extended Gold Sample was constructed to be relatively free from non-extended or non-astrophysical sources, but our curation was deliberately liberal so that borderline cases could be handled more carefully on a case-by-case basis. Having constructed the Gold Sample, we performed this more careful analysis on those objects whose calibrated photometry indicate that they are especially red.

As discussed in Section 2.6, we have performed magnitude corrections using the photometry provided by the *WISE* pipeline. For every source in the Extended Gold Sample we now have photometry using four different photometric systems (i.e. MPRO (profile), MAG (aperture

corrected magnitude), CMAG (Corrected Magnitude, see Section 2.6), and GMAG (elliptical aperture)). While the corrected magnitudes are reliable for most sources, there are special cases where a different photometric system may yield more reliable results. Given this, we have measured γ , T_{waste} , and $L/(4\pi d^2)$, (see Section 4.0, and Paper II) in each of the four different photometric systems.

To ensure that our choice of photometry does not cause us to miss any red sources, we selected from the Extended Gold Sample all sources with $\gamma \geq 0.25$ in any of the photometric systems. This identified a total of 3,145 sources. We used our collected imaging, grading, and literature search results (Section 4.3) to carefully and visually vet this sample to identify and remove the most obvious contaminants, mostly nebulosity and saturated stars that survived our very liberal curation of the Extended Gold Sample. We identified and removed 366 obvious contaminants, reducing our list to 2779 objects.

We found that in a small percentage of cases, especially with blended sources, an extended source is broken up into two or more components in the All-sky catalog. In these cases we choose the entry coordinates closest to the extended source center and the photometric system that best captures the true magnitudes of the extended source. In some cases, the W3RCHI2 value of the catalog entry centered on an extended source is below 3 because of the details of how the All-sky catalog breaks up composite sources.

We segregated this sample into four different categories and determined which photometric system best fits the source in question:

- Extended Source: Source is truly extended in the *WISE* images
- Point Source Galaxy: Source appears to be a galaxy from O/IR imaging or other sources, but appears unresolved in the *WISE* imagery, despite having a high W3RCHI2 value.
- Point Source Star: Source appears to be stellar in nature.
- Junk: Source is a contaminant, should not be in any catalog of real astrophysical sources.

In addition to classifying these sources as described above, we also determine which photometric system best estimates the true photometry of the given source. We use the following convention to indicate the best possible *WISE* photometry in the source tables:

- 0: MPRO (Profile fit photometry)
- 1: MAG (Aperture-corrected magnitude)
- 2: CMAG (Corrected magnitude)
- 3: GMAG (2MASS XSC elliptical aperture).

Using these conventions we identify 1296(46.7%) classified as Extended, 974(35%) classified as unresolved galaxies, 263(9.4%) classified as stellar, and 246(8.9%)

TABLE 3
FREQUENTLY ENCOUNTERED CATALOGS MATCHING RED EXTENDED *WISE* SOURCES

Reference	Catalog Description
Cotton et al. (1999)	Arcsecond Positions of Uppsala General Catalog (UGC) Galaxies
Falco et al. (1999)	The Updated Zwicky Catalog (UZC)
Lauberts & Valentijn (1988)	The surface photometry catalogue of the ESO-Uppsala galaxies
Lavaux & Hudson (2011)	The 2M++ galaxy redshift catalogue (69,160 galaxies)
Lawrence et al. (1999)	The QDOT all-sky IRAS galaxy redshift survey
Mitronova et al. (2004)	The 2MASS-selected Flat Galaxy Catalog (18,020 disc-like galaxies)
Patuel et al. (2000)	Positions for 17,124 galaxies including 3301 new companions of UGC galaxies
Ramella et al. (2002)	The UZC-SSRS2 Group Catalog (1168 galaxy groups)
Saunders et al. (2000)	The PSCz catalogue (15,411 IRAS galaxies)
Takase & Miyauchi-Isobe (1984)	KISO survey for ultraviolet-excess galaxies.
Wang & Rowan-Robinson (2009)	The Imperial IRAS-FSC Redshift Catalogue (60,303 galaxies)

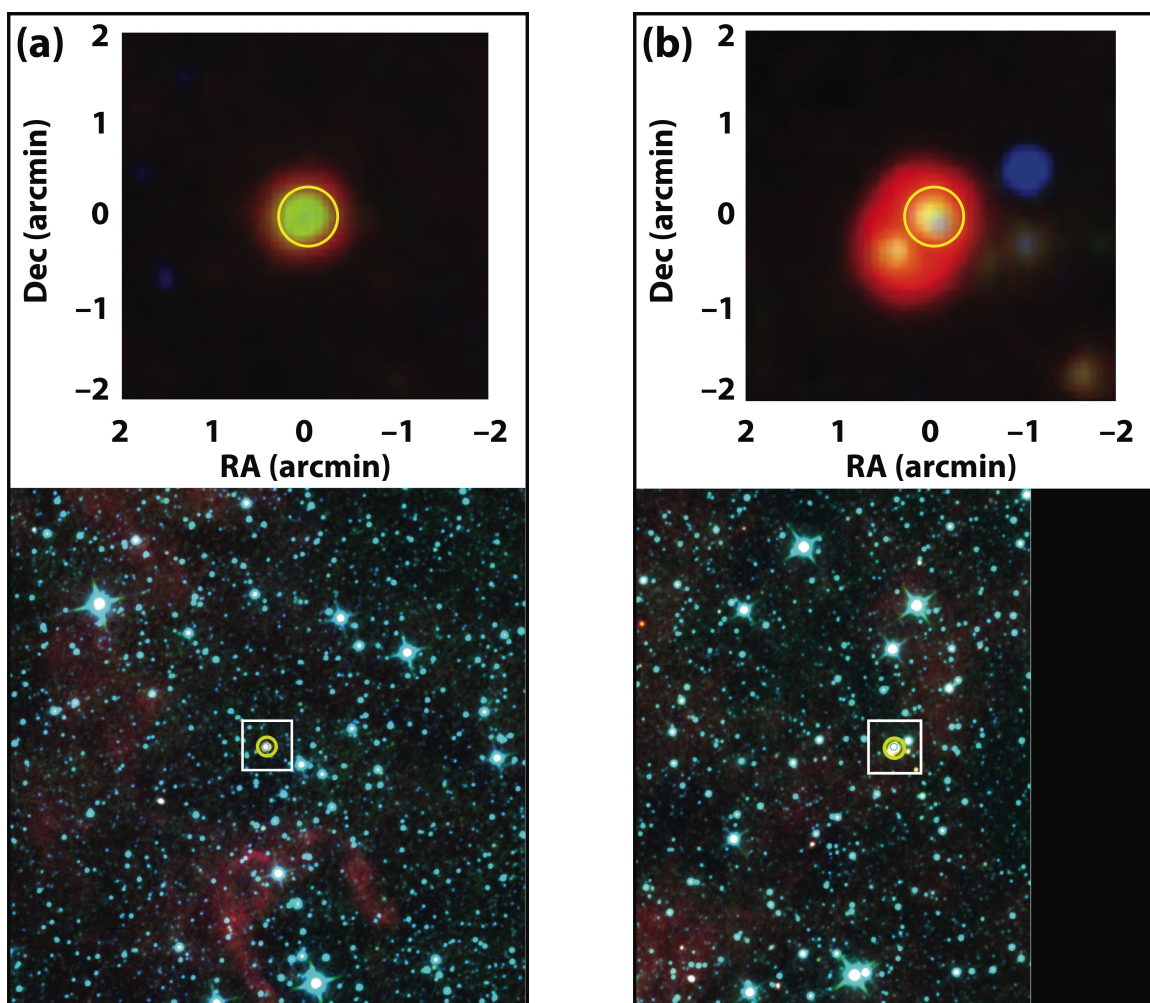


FIG. 14.— Left (a): Source W224436.13+372533.7, an example of an isolated red source given an A grade. Right (b): Source W043329.56+645106.5, an unusual cluster of sources discovered by our search, also given an A grade. Top panels show the color-composite *WISE* $2' \times 2'$ “postage stamp” images from our “at-a-glance” charts (red = W4, green = W3, blue = W1+W2), while bottom panels show the same sources in the wider $30' \times 30'$ *WISE* atlas images (red = W3, green = W2, blue = W1).

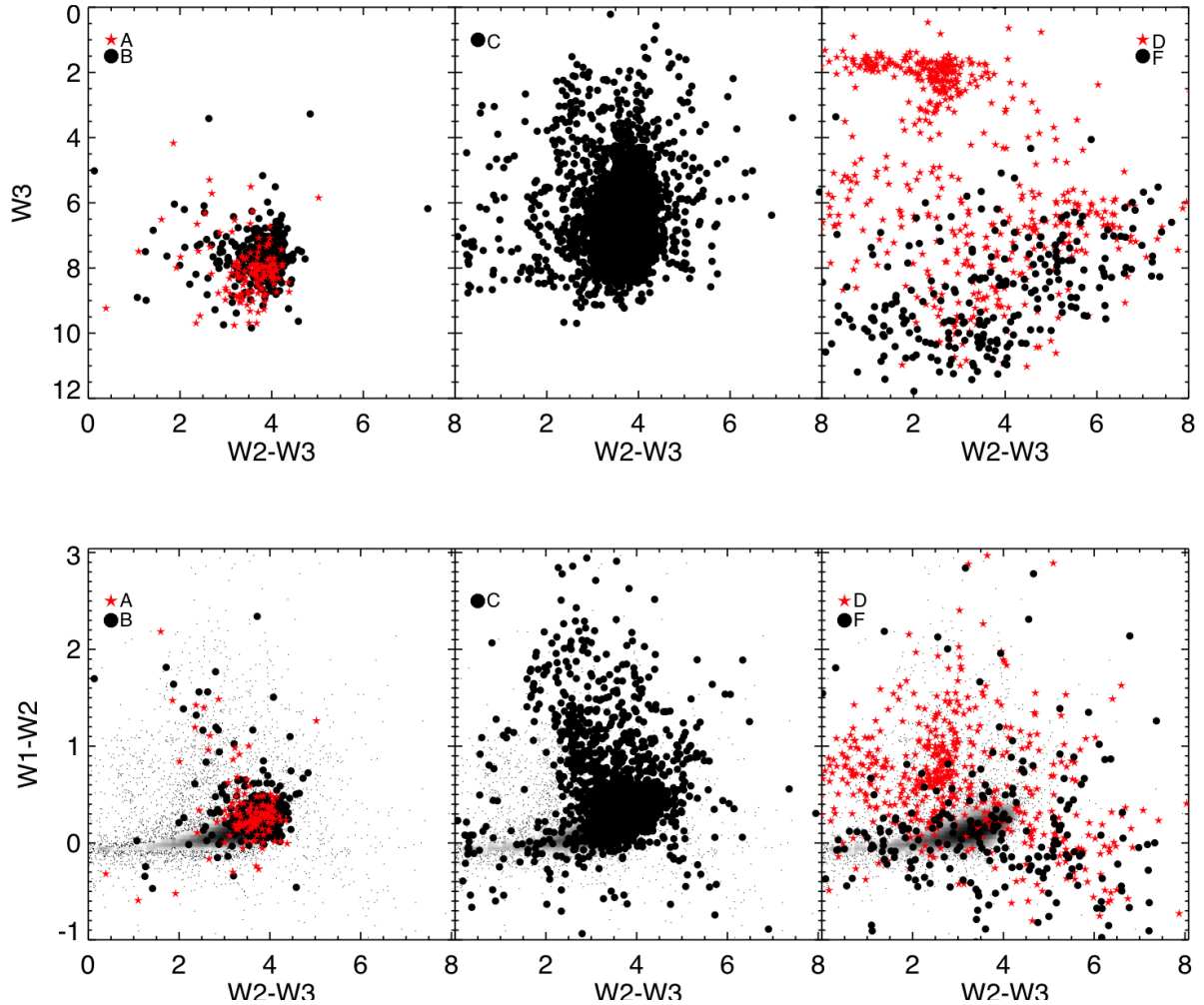


FIG. 15.— Color-magnitude diagrams (top) and color-color diagrams (bottom) for W3 Extended Gold sample sources which have been carefully vetted and classified as described in Section 4.3. Sources with no or little literature presence (grades A and B, respectively) are in the left panels; well-studied sources (grade C) are in the middle; saturated stars and artifacts (grades D and F, respectively) are on the right. Unsurprisingly, grade A and B sources (i.e. sources with little presence in the literature) are typically faint, and grade D and F sources have extreme colors and magnitudes (indicating that they are artifacts of the instrument or the analysis pipeline strongly affecting some bands but not others). The density of all W3 Extended Gold Sample sources is indicated in grayscale in the bottom panels. We use plots such as this to ensure that we understand the effects of making cuts based on our grading scheme.

classified as junk. Of the Extended sources, 563 have $\gamma > 0.25$ in the photometric system most appropriate for that source. These compose our W3 Extended Platinum Sample of real, extended, red sources in *WISE*.

5.2. *Platinum Sample Published Catalog*

We present a catalog of 563 sources deemed to be extended and real in the *WISE* $12\mu\text{m}$ filter and identified as the Platinum Sample as a FITS file associated with this manuscript. This list of sources have also been selected as those having $\gamma \geq 0.25$ in the preferred photometric system. Table 4 gives the detailed parameter description for this electronic catalog. For brevity, we present a minimal number of parameters representing the most important measurements for these sources, and the *WISE* identifier so that users may cross-reference our catalog to the *WISE* All-sky or ALL-*WISE* catalogs. Presented in this parameter list are the coordinates, optimal *WISE* photometry and the photometric system used (see Section 5.1), the AGENT parameters, and pertinent information derived from the SIMBAD database. Tables 6–9 have been derived using this catalog.

6. EXTREME EXTENDED OBJECTS IN THE PLATINUM SAMPLE

6.1. *Extreme WISE Colors*

The *WISE* filter system allows for the measurement of 6 different photometric colors, i.e. W1-W2, W2-W3, etc. In Table 6, we present a list of the 10 reddest (per color) objects contained within the Extended Platinum Sample. These objects have been ordered by decreasing “redness”, so that the 10th object in the list represents the 10th reddest object within the color explored.

The most extreme MIR objects in the high latitude sky ($|b| \geq 10$) appear to be dominated by PNs. Other objects with extreme colors include a pair of comets, three YSOs, a handful of Type II Seyfert galaxies, two uncataloged sources in the LMC that escaped our mask of that region, and some objects we discuss in Section 6.2.

Since this study is primarily interested in finding ETIs of extra-galactic origin we present Table 7, which is a list of the 10 reddest (per color) high latitude extragalactic objects seen in the Extended Platinum Sample. We find that the colors of galaxies are in general not as extreme as Galactic sources. Most of the galaxies on this list are Grade C, meaning that their nature has been identified in the literature.

Table 7 is dominated by galaxies classified in SIMBAD as AGN of various stripes, which is unsurprising since those galaxies are often characterized by their extreme MIR emission. AGN are thus, as expected, our primary confounders in our waste heat search for K3 civilizations.

6.2. *Extreme γ*

In the AGENT formalism (Section 4.1, Wright et al. (2014a)) the parameter γ represents the fraction of starlight reemitted in the MIR, at temperature T_{waste} . We have measured maximal values for this parameter assuming that there is no dust in any of our sources,

and that their underlying stellar population is that of an old elliptical galaxy (so, virtually dust-free). Since this is the parameter of interest in searches for alien waste heat, we have sorted the Extended Platinum Sample by this parameter. We present the top 50 such galaxies in Table 8.

The galaxy with the highest measured γ ($= 0.85$) is NGC 4355 (=NGC 4418), which is also has the most extreme colors in four of the six *WISE* color combinations. It is a well-studied Type II Seyfert galaxy in the Virgo cluster with a (W1-W4) color of 10.19, with the extreme MIR emission being due to the AGN.

The second source on our list is IRAS 04259-0440, a marginally resolved galaxy with modest presence in the literature. It has been studied in the context of being a Seyfert galaxy or LINER Wu et al. (2011), so we are convinced that the MIR emission is understood. Nonetheless, given the extreme nature of this galaxy’s infrared emission, this galaxy would appear to warrant more attention than it has received to date.

The third galaxy in our list is the well-studied Arp 220, the quintessential local starburst galaxy and a known active galaxy. Fourth and fifth are UGCA 116 and IRAS F20550+1655-SE, both pairs of interacting galaxies. In all three cases, the extreme MIR colors are clearly due to star formation triggered by galaxy interactions.

6.3. *Extreme Objects New to Science*

One of the primary objectives of this investigation is to search and identify the most rare and extreme sources in the high latitude infrared sky. The majority of the sources in our tables have already been discovered and discussed in various articles, but there are still a small number of objects not previously discovered or discussed in the literature.

In Table 9 we present 3 objects ($\gamma \geq 0.25$) classified as As, meaning that they are essentially new to science. In this section we also discuss an extreme and apparently anomalous object that we gave a B grade, IRAS 15553-1409, and a particularly interesting lower- γ grade A source.

6.3.1. *IRAS 04287+6444: An Unusual Cluster of MIR Sources With no Optical Counterparts*

Our most unusual objects are associated with IRAS 04287+6444. The brightest of these sources is slightly blended, which complicated our magnitude corrections, giving our source an erroneously high γ value before our quality checks corrected the error. This blending also triggered the high W3RCHI2 value that suggested this was extended source. There appear to be at least seven very red point sources clustered in this region in all. We identify and number four fainter sources in Figure 16 (Bottom right); the other three or more all contribute to the brighter blend in the NE.

NED reports five entries within $2'$ of these sources’ positions. The two nearest detections are from the 2MASS Extended Source Catalog (see below), and the third nearest entry is the IRAS counterpart to this source. The other two NED entries are a ROSAT detection (1WGA J0433.4+6451 Voges et al. 1999) centered $\sim 33''$ away (outside the $20''$ astrometric precision of ROSAT), and

TABLE 4
PLATINUM SAMPLE PUBLISHED CATALOG

Parameter	Type	Entry	Description
DESIGNATION	STRING	J190101.24-181215.0	<i>WISE</i> Designation
NAME	STRING	PNA6651	SIMBAD Identifier
GRADE	STRING	C	Grade (see Section 4.3)
SIMBAD_TYPE	STRING	PN	Object Type
R.A.	DOUBLE	285.25520	Right Ascension [degrees]
Decl.	DOUBLE	-18.204188	Declination [degrees]
W1BEST	FLOAT	15.4980	W1 optimal photometry [mag]
W2BEST	FLOAT	13.889	W2 optimal photometry [mag]
W3BEST	FLOAT	9.0770	W3 optimal photometry [mag]
W4BEST	FLOAT	3.0690	W4 optimal photometry [mag]
PHOT_SOURCE	INT	1	Photometric System, see Section 5.1
TWASTE	FLOAT	72.923	Waste heat temperature [K]
GAMMA	FLOAT	0.99294	AGENT parameter γ
BOL_FLUX	FLOAT	255.83	Bolometric flux [L_{\odot}/pc^2]

the 1.4 GHz radio source NVSS J043322+645120 (Condon et al. 1998) centered $\sim 0.8'$ away (consistent with being associated with our source).

Strauss et al. (1992) included the IRAS center in their optical spectroscopic survey, and identified it as “cirrus or dark cloud,” although they note that a significant number of such entries may in fact be galaxies. This non-detection is not surprising given the lack of optical counterpart to these objects.

We have found a serendipitous archival *Spitzer* MIPS image of these sources, taken because they are within $15'$ of HD 28495, a target observed with IRAC as part of the FEPS program (Meyer et al. 2006). Figure 17 shows how the superior resolution of this 22μ imagery reveals substructure to the SE component of the bright blend, and many sources undetected by *WISE* (without color information, it is unclear whether these sources are associated with IRAS 04287+6444).

Objects #1 and #3 are barely detected in the WISE images (not appearing in the W4 band at all) and thus provide little clues as to their true nature, but appear to be fainter versions of the other red objects, with similar colors. Objects #2 and #4 appear cleanly detected in all four bands.

The angular proximity to HD 28495 is intriguing, but these are likely unassociated since a common distance at 25 pc van Leeuwen (2009) would imply a projected separation of $\sim 2 \times 10^4$ AU. Nonetheless, the lack of optical counterpart complicates efforts to rule out this scenario from proper motion.

One possibility is that this is a previously uncataloged moderate-latitude ($b = 11.5^\circ$) dark cloud, and that these are an embedded cluster of young stellar objects or protostars. Figure 18 shows the 2MASS imagery for this region, which has significantly better angular resolution. This NIR imagery reveals that the brightest source in the *WISE* imagery comprises at least three sources, only one of which is evident in J band. Supporting this interpretation, Yang et al. (2002) detected CO (J=1 \rightarrow 0) emission in the direction of the IRAS source¹⁰ with LSR radial

velocity -13.27 km/s and FWHM 3.4 km/s, implying a molecular cloud exists in this direction at a kinematic distance of 840 pc (and thus a height of ~ 170 pc below the Sun’s position in the plane).

If the sources are extragalactic, the most natural explanation is that they are members of a galaxy cluster. Edelson & Malkan (2012) identified the IRAS source as having a modest chance ($\sim 50\%$) of being an AGN of some flavor based on the *WISE*, 2MASS, and X-ray fluxes, however the X-ray detection may be unassociated, and it appears this probability does not incorporate the fact that the source has no optical counterpart or that it is not isolated.

The lack of optical counterpart could be due to redshift and internal extinction. A significant population of high redshift ($z > 2$) and more luminous ($L_{IR} > 10^{13}L_{\odot}$) Dust Obscured galaxies (called Hot Dust-obscured Galaxies, or “Hot DOGs”) have recently been identified by the WISE survey, (see Eisenhardt et al. 2012; Wu et al. 2012; Bridge et al. 2013; Stern et al. 2014, for a detailed discussion of these types of objects). Indeed, the strong 22μ emission for these objects are reminiscent of Dust Obscured Galaxies (DOGs), either local ($z \sim 0$) (Hwang & Geller 2013) or at high redshift ($z \geq 2$) (Dey et al. 2008).

However, our objects are inconsistent with hot DOGs since hot DOGs tend to have very little or no emission in the shorter WISE bands. And such extreme examples of dusty galaxies are not typically highly clustered as our sources are.

We tentatively favor the interpretation that this is a cluster of young stellar objects embedded in and heavily extinguished by their parent molecular cloud. We are intrigued by these objects, and we hope that spectroscopic observations can and will reveal their true nature in the future.

6.3.2. *WISE J224436.12+372533.6: A new MIR-bright galaxy*

presume that Yang et al. erroneously transposed the “Association” values for these entries. If, instead, it is the target names that are transposed, then the appropriate LSR radial velocity for IRAS 04287+6444 is 6.91 km/s, the FWHM is 4.3 km/s, and no kinematic distance is available.

¹⁰ The “Association” field from Table 2 of Yang et al. (2002) for IRAS 04287+6444 confusingly reads “HL Tau”. HL Tau itself appears in the table two entries prior, where the “Association” field reads “04288+6444,” apparently a typo for 04287+6444. We

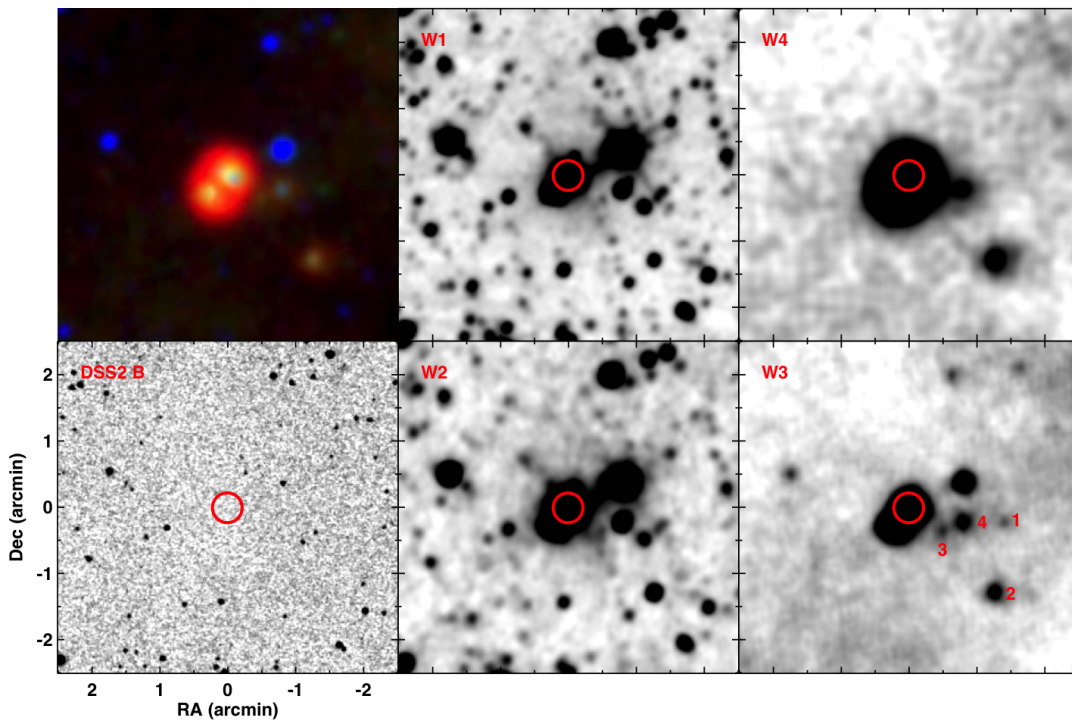


FIG. 16.— Six views of the extremely red source IRAS 04287+6444 (WISE J043329.55+645106.5). A red circle indicates the common position of the WISE emission peak in all six panels. There is no hint of any emission in the optical (B band, lower left). *WISE* reveals a large number of sources in the region in W1 and W2 (top and bottom middle), and a pair of extremely bright, blended sources in W4 (upper right). The color composite image (upper left) shows that there are also four, fainter but also very red objects to the southwest of the primary pair. We label these four sources in the W3 image (lower right).

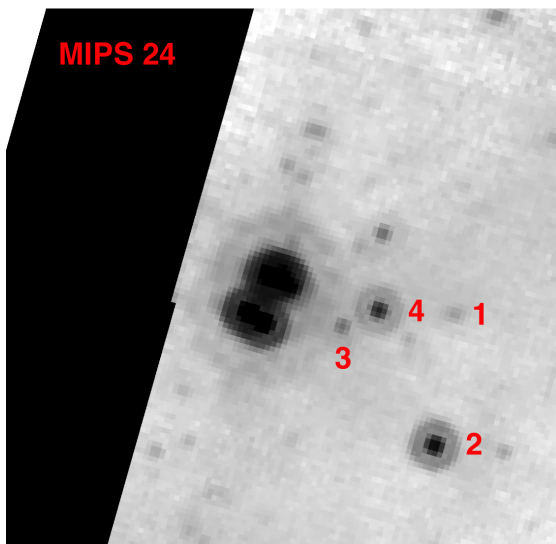


FIG. 17.— Serendipitous archival MIPS imagery of IRAS 04287+6444. The bright *WISE* source (which shows substantial substructure here) and the four fainter *WISE* sources are all detected in this 22μ image.

We gave the object WISE J224436.12+372533.6 (shown in Figure 19) an A grade because it has no presence in the astronomical literature beyond having been noted in the 2MASS Extended Source Catalog. It is MIR bright and red, and DSS and 2MASS imaging shows what appear to be a galaxy. It is just barely detected by IRAS (it appears in only two bands in the IRAS Faint Source catalog (Moshir, M. et al. 1992)), and so may have evaded prior notice for that reason. It also appears as a 1.4 GHz source in the NRAO VLA radio survey Condon et al. (1998). This source deserves further study to understand its superlative nature.

6.3.3. IRAS 16329+8252: An MIR-bright galaxy at $z=0.04$?

We give this source an A grade because it has virtually no presence in the literature beyond a single low resolution spectrum by Chen et al. (2011). If their identification of the emission lines in this spectrum is correct, then it is a galaxy at $z = 0.039$. Its strong MIR emission suggests large amounts of star formation, possibly triggered by the disturbance of a nearby neighbor (see Figure 20).

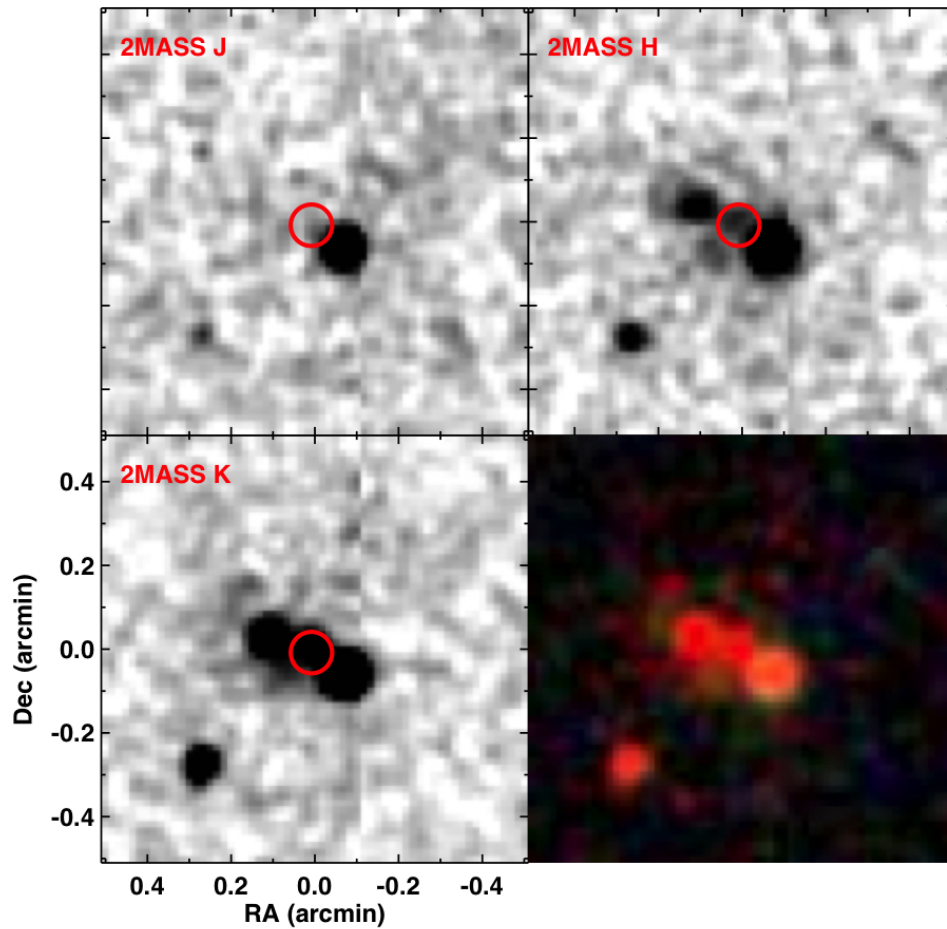


FIG. 18.— Four closer-in, NIR views of the extremely red source IRAS 04287+6444 (WISE J043329.55+645106.5) from 2MASS. A red circle indicates the common position of the WISE emission peak in the three single-band panels. Note the change in angular scale with respect to Figure 16. The K band image (lower left) reveals that the bright *WISE* source comprises at least three sources. Of these, only the NE and SW sources are apparent in H band (upper right), and only the SW shows a J band counterpart (upper left). The more distant SE object, responsible for making the *WISE* source appear extended, is detected in all three bands. The color composite (lower right) shows that all four sources have extremely red NIR colors.

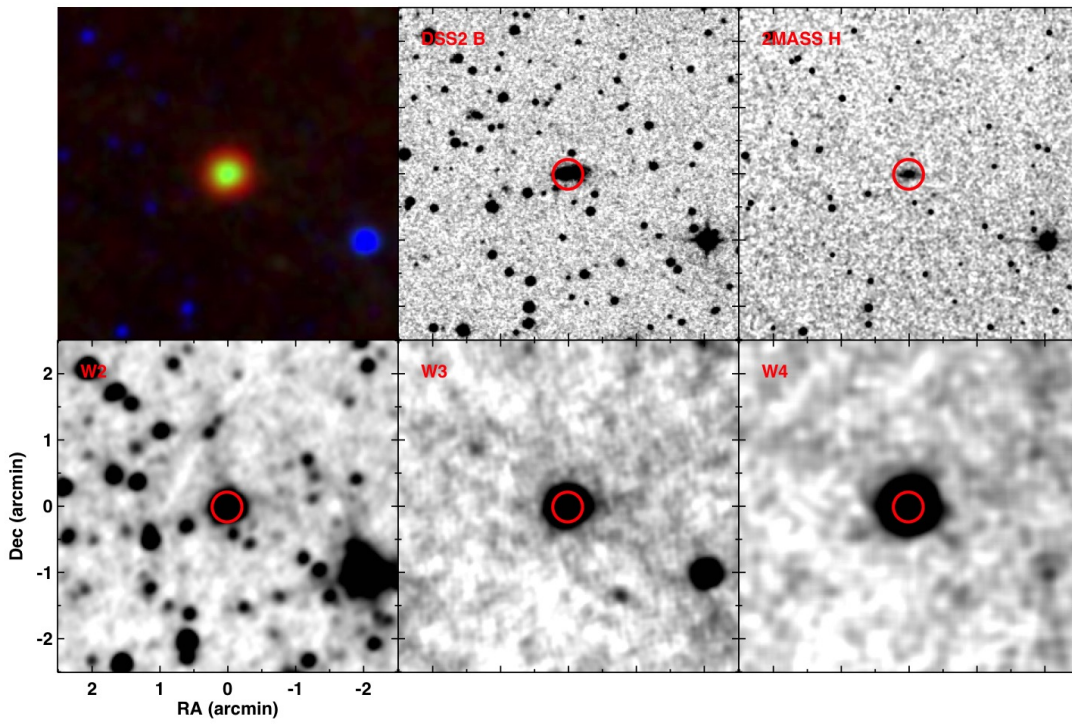


FIG. 19.— The previously unstudied but MIR-bright galaxy WISE J224436.12+372533.6. It was only barely detected by IRAS, but is easily detected by *WISE* as an extremely red MIR source.

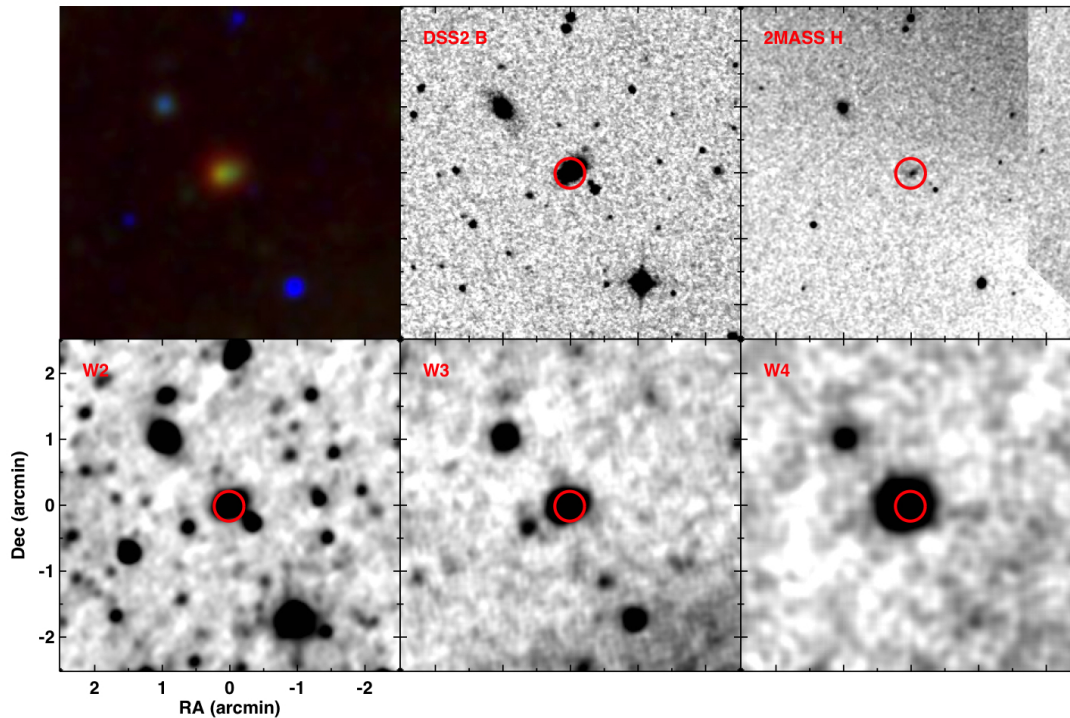


FIG. 20.— Six views of the extremely red source IRAS 16329+8252. A red circle indicates the common position of the WISE emission peak in all six panels. The MIR morphology (upper left, where red = W4, green = W3, blue = W1+W2) is consistent with the optical B band (upper middle), although the shorter WISE bands (W2, lower right) appear slightly offset to the west, consistent with the H band imagery (upper right). The W3 and W4 band imagery appear very slightly extended. This is apparently a very MIR-bright $z=0.039$ galaxy, possibly disturbed by a neighbor to the northeast, or along the line of sight.

6.3.4. *WISE J073504.83-594612.4: a pair of merging galaxies?*

We graded the source WISE J073504.83-594612.4 (Entry 2 in Table 9) A because it has virtually no presence in the literature, appearing only in a handful of photometric catalogs, including the 2MASS extended source catalog. It has no IRAS counterpart. It appears to be extragalactic.

The WISE color image (Figure 21) shows little structure; it is barely extended in W3 and W4. The H band and W2 imagery, which presumably trace the stellar populations of the bulges of the galaxies in this imagery, reveals two sources, one at the position of the WISE source and one $\sim 20''$ to the north. The DSS B band image shows significant structure between these positions, suggesting that this is a disturbed or merging galaxy pair. The bright W4 emission suggests that this disruption is generating significant star formation in the southern galaxy.

6.3.5. *IRAS 15553-1409: a large nebula of dust from a Be shell star?*

The infrared source IRAS 15553-1409 is the reddest or second reddest source in four of the six WISE colors. We

give this source a B grade because it has virtually no presence in the literature, beyond Carballo et al. (1992), who identify it as a potentially “evolved Galactic object.” WISE imagery reveals it to be a MIR-bright nebula associated with the classical Be star 48 Librae. Figure 22 shows that the MIR morphology and colors are similar to that of reflection nebulae, but in this case there is no apparent emission in the optical.

48 Librae is known to be a classical Be shell star (e.g. Jaschek & Jaschek 1992) and a member of the Sco-Cen Association. It has a distance of ~ 140 pc (van Leeuwen 2009), expansion velocities of 25 km/s (Hoffleit & Warren 1995), and age < 20 Myr (Eric Mamajek, private communication¹¹ and references therein.) It is sometimes listed in the literature as a giant star, but this is likely because its rapid rotation gives it an anomalously low surface gravity, complicating its spectrally derived luminosity classification.

This source is superlative because of its extreme MIR colors and extent, although this is a byproduct of its proximity; similar Be shell stars at greater distances

¹¹ <https://www.facebook.com/jason.wright.18062/posts/10204670796112674>

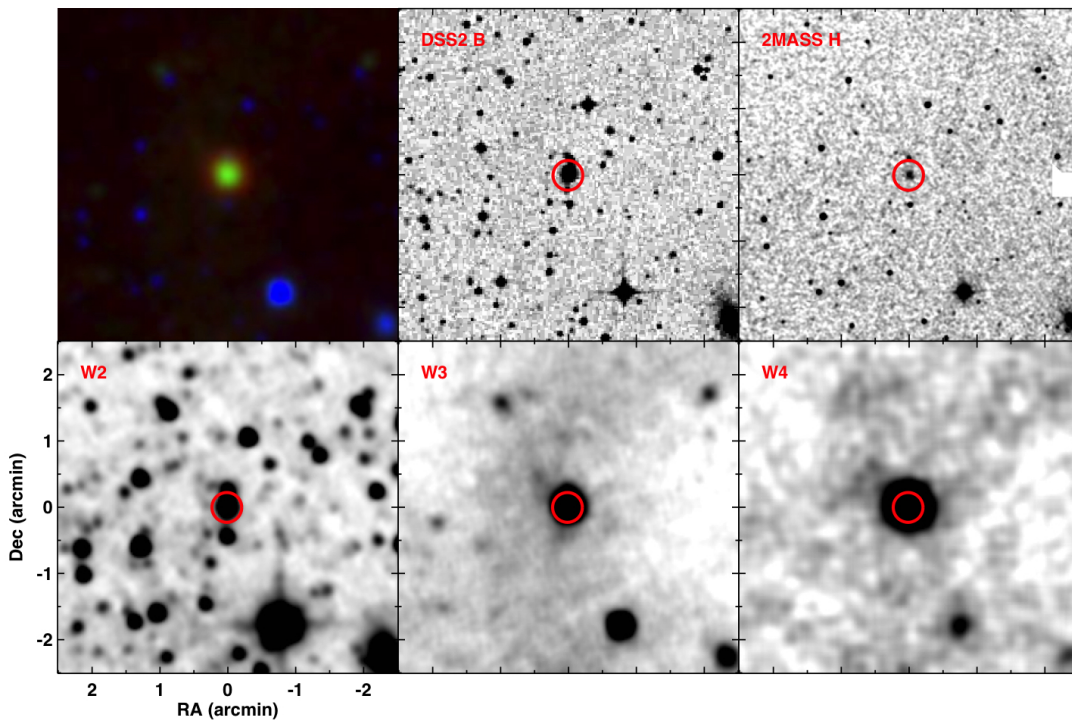


FIG. 21.— Six views of the extremely red source WISE J073504.83-594612.4. This source has no known IRAS counterpart. The *WISE* color image (upper left, where red = W4, green = W3, blue = W1+W2) shows little structure; it is barely extended in W3 and W4 (lower middle and right). The H band image (upper right) and W2 image (lower left) reveals two sources, one at the position of the *WISE* source and one $\sim 20''$ to the north, which are perhaps the bulges of a pair of galaxies. B band shows a possible bridge of material between the two H band sources, indicating that this may be a pair of merging galaxies.

would not be resolved.

Adams et al. (2013) notes that the infrared excesses of main sequence stars typically have one of four origins: circumstellar debris disks, protoplanetary and protostellar disks around very young stars, “cirrus hot spots” caused by the illumination of ambient interstellar dust, and the excretion disks of classical Be stars.

Cirrus hot spots (Adams et al. 2013; van Buren & McCray 1988) can be simple reflection nebulae (the “Pleiades phenomenon,” Kalas et al. 2002) or the result of bow-shocking by the star’s wind or radiation as it moves through the ISM (e.g. van Buren & McCray 1988; Povich et al. 2008; Everett & Churchwell 2010). Inspection of the morphology of typical reflection nebulae (including that of the Pleiades themselves and those discovered by Kalas et al. (2002)) shows that 48 Librae does not appear to be a typical example. The 48 Librae nebula has no optical counterpart, suggesting that the 22 micron emission is thermal, and appears to have symmetries about the position of the star, suggesting that it has some connection to the star beyond being illuminated by it (see Figure 23).

The most likely explanation of this nebula is that it is therefore a ring or bow shock. The bow shock and ring

interpretations are complicated by the fact that, despite being a Sco-Cen Association star, 48 Librae does not appear to be embedded in a region of high density gas and dust, and that its space motion is not large.

The proper motion of 48 Librae is SW $((\mu_\alpha, \mu_\delta) = (-12.44, -16.73)$ mas/yr van Leeuwen 2009), which is not in the direction of the brightest sources of emission, but it appears that most of this apparent motion is actually due to motion of the Sun with respect to the local standard of rest. Correcting for the solar motion (using radial velocity 7.5 ± 1.8 km/s (Gontcharov 2006) and the LSR of Mihalas & Binney (1981)), the proper motion is still roughly SW $((\mu_\alpha, \mu_\delta) = (-2.4, -0.9)$ mas/yr), corresponding to an LSR space velocity of 4 km/s, with an error of a few km/s from our LSR correction.

Further complicating the bow shock interpretation is that both sides of the 48 Librae nebula have similar arcs consistent with being portions of rings inclined $\sim 20^\circ$ from edge-on, and centered on the star.

Given these difficulties with the typical bow shock and ring models, we suggest that the nebula have originated with the star itself. Classical and shell Be stars are not typically considered to be significant sites of dust formation or sources of MIR excess (Rivinius et al. 2013),

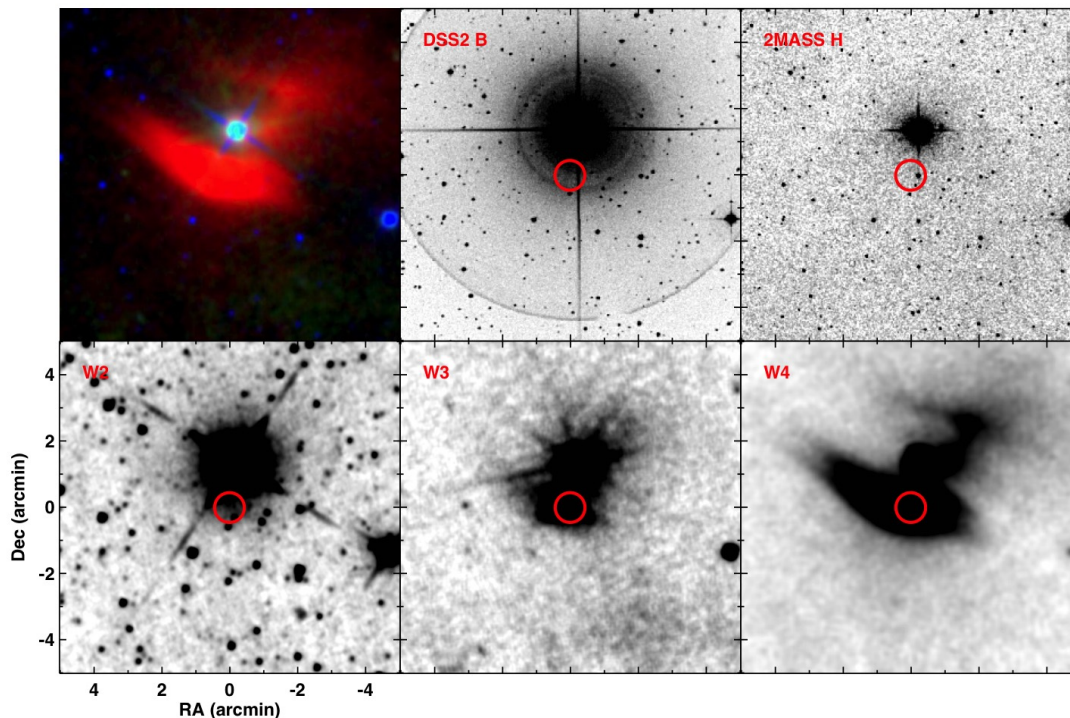


FIG. 22.— Six views of the extremely red source IRAS 15553-1409 (WISE 1558-1418). A red circle indicates the common position of the WISE emission peak in all six panels. The bright point source is the Be star 48 Librae. The MIR morphology (upper left, where red = W4, green = W3, blue = W1+W2) is typical of a reflection nebula, but there is no emission obvious in the optical (B band, upper middle). The NIR (H band, upper right) and W2 bands (lower left) appear unremarkable. The brightest part of the cloud is apparent in W3 (lower middle) and large amount of diffuse emission are obvious around the star in W4 (lower right).

although NIR excesses, presumably due to circumstellar dust, are common, and many unclassified Be stars are known to have MIR excesses (e.g. Miroshnichenko & Bjorkman 2000; Lee et al. 2011; Miroshnichenko et al. 2001). 48 Librae has one of the larger and stronger disks known among classical Be stars (T. Rivinius, private communication).

Since 48 Librae is known to have shells, a time variable disk (Štefl et al. 2012), and significant mass loss, it is reasonable that some of this shell material would condense into dust near the star before being lost (Lee et al. 2011). The nebula is not too large for this: the nebula has an angular size of order a few arcminutes, which at the distance of 48 Librae (~ 150 pc) corresponds to $\sim 15,000$ AU. The expansion velocity of the shells is 25 km/s, yielding a characteristic timescale of $\sim 30,000$ yr, significantly shorter than the Be phase of a star.

So, we may be seeing shocked dust where the shells (really rings) of excreted material collide, either with the ambient ISM or with previously ejected material. If so, then we expect the rings we observe in the nebula to have a rough correspondence to the geometry of the excretion disk. The rings (which we fit by eye) have an inclination of 70° (i.e. 20° from edge-on), and a position

angle of 72° . The actual inclination of the excretion disk must be $\gtrsim 65^\circ$ (because it shows absorption lines from the disk, T. Rivinius, private communication), and the actual position angle is known from interferometry to be $50^\circ \pm 9^\circ$ (Štefl et al. 2012), consistent with our rings at $1-2\sigma$, within the rough precision with which we can define them.

Alternatively, we may be seeing excreted dust being illuminated by UV radiation from 48 Librae itself, although this interpretation is complicated by the lack of apparent optical scattered light, and by the patchiness of the emission.

It is unclear if the nebula contains more dust than could be plausibly explained by the currently observed mass loss rate, but of course 48 Librae could have had episodes of higher mass loss rates in the past.

This object may be revealing to us that Be shell stars are, in fact, common sites of dust generation. This phenomenon warrants further study.

7. UPPER LIMITS ON THE ENERGY SUPPLIES OF TYPE III KARDASHEV CIVILIZATIONS

7.1. Limits on energy supplies as a fraction of stellar luminosity

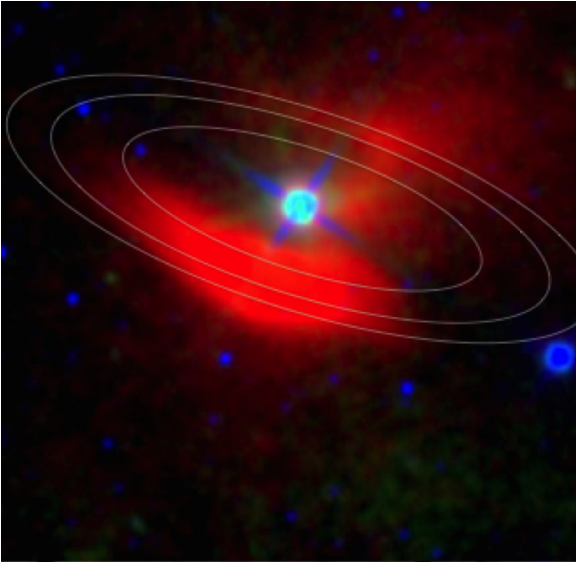


FIG. 23.— A *WISE* color composite of the 48 Librae nebula, with ellipses overlain to illustrate the common symmetries of the arc structures in the nebula. The ellipses describe concentric rings centered on the star inclined 19° from edge-on. The physical size of the nebula is $\sim 15,000$ AU.

We can use those sources in our study with the largest amounts of thermal emission to set an upper limit for waste heat emission among the galaxies we have surveyed. We have found no sources with $\gamma > 0.85$, and the 50 galaxies we have found with $\gamma > 0.5$ appear to have natural origins to most of their MIR emission, although we have not rigorously verified this.

These values for γ were calculated under the assumption that our target galaxies are composed of only two components: an old stellar population, and alien waste heat originating entirely from reprocessed starlight. Since real galaxies have other sources of MIR emission, these numbers are upper limits on the integrated alien waste heat emitted by these galaxies.

Our assumption that the origin of the alien waste heat is intercepted starlight (i.e. $\gamma = \alpha$, where α is the fraction of starlight intercepted, see Section 4.1) means that we have assumed that the flux in the W1 and W2 bands, which in our model constrain the total stellar luminosity, does not include the starlight lost to alien factories. If, instead, we assume that all alien waste heat is generated by other means and that only a negligible fraction of starlight is occulted ($\alpha \sim 0$), then we would infer a higher value for the fraction of starlight emitted as waste heat. Specifically, our limiting values of $\gamma = 0.85$ and 0.5 correspond to $\gamma_{\alpha=0} = 5.7$ and 1 (see Section 3.2 Wright et al. 2014a).

In other words, we have shown that there are no galaxies resolved by *WISE* with MIR luminosities consistent with alien energy supplies in excess of 5.7 times the starlight in their galaxies (i.e. we have ruled out $\gamma = \epsilon > 5.7$). If all of 50 galaxies in our list turn out to have purely natural origins to their emission, then this upper limit drops to $\gamma = \epsilon < 1$.

If we assume that any large alien energy supply will be based on starlight (that is, $\gamma \sim \alpha$ and $\epsilon \sim 0$), then our

upper limit is much tighter: no resolved galaxies exist in our search area with more than 85% of their starlight reprocessed by alien factories, a limit which will drop to 50% when our 50 high- γ galaxies are more carefully vetted.

Translating these numbers into physical units (erg s^{-1}) will require a more detailed modeling of the stellar and nonstellar components of the galaxies we have surveyed, a project which is beyond the scope of this paper. We hope to pursue this in a future paper.

7.2. Number of galaxies surveyed

Translating our upper limits into an upper limit on the frequency of K3's requires knowledge of the number of galaxies we have effectively surveyed. We cannot use our Gold or Platinum Samples to estimate this number because they included color cuts to remove stars that also removed elliptical and other dust-free galaxies. Even if we had imposed no such cuts, there are many galaxies that would be resolved in the W3 band if they were MIR bright, but are unresolved — or in some cases undetected — in *WISE* because their MIR surface brightness is below the *WISE* detection limits.

To estimate the number of galaxies that *would have been included* in our sample *if* they had $\gamma > 0.5$, we can use the number of sources in the W1 and W2 bands. The W1 band, in particular, has better angular resolution than W3, and is primarily sensitive to stellar photospheres, so is in many ways a clean band for estimating the angular extent of galaxies around which alien factories might reside.

One concern with using *WISE* data for this purpose is that, as we have seen, the source counts include many non-galaxies (including artifacts), and many point sources have erroneously large values of RCHI2. To mitigate this, we have used the 2MASS Extended Source Catalog (XSC), which is relatively clean of point sources and is composed almost entirely of galaxies.

We first cross-matched *WISE* to the 2MASS XSC, and selected only those sources with $|b| \geq 10$. We then examined the NIR properties of MIR-red galaxies in the 2MASS XSC by examining the relationship between the WXRCHI2 values for the W1 and W2 bands and the W3RCHI2 parameter, which we used for the Platinum sample. We restricted our analysis to 9,589 matched sources with $(W1-W3 \geq 3.8)$ for the W1RCHI2 analysis, and 14,927 sources with $(W2-W3 \geq 3.5)$ for the W2RCHI2 analysis.

The left hand panels of Figure 24 show the relationship between the W1RCHI2 and W2CHI2 parameters (which describe the degree to which galaxies are resolved in those bands, see Section 2.1) and the vs. W3RCHI2 parameter we used to define a source as “extended” in our survey.

These panels show that, for the red sources we used to construct this figure, we can use $W1RCHI2 > 12$, and $W2RCHI2 > 3$ as proxies for our actual criterion $W3RCHI2 > 3$. Using the full *WISE*-2MASS XSC cross-matching (that is, not imposing any color cuts), we find 1,589,099 sources common to both catalogs. Of these, 1,463,781 have $|b| \geq 10$. Of these, 111,617 have $W1RCHI2 \geq 12$ and 104,039 have $W2RCHI2 \geq 3$. These figures are consistent, suggesting that we have surveyed

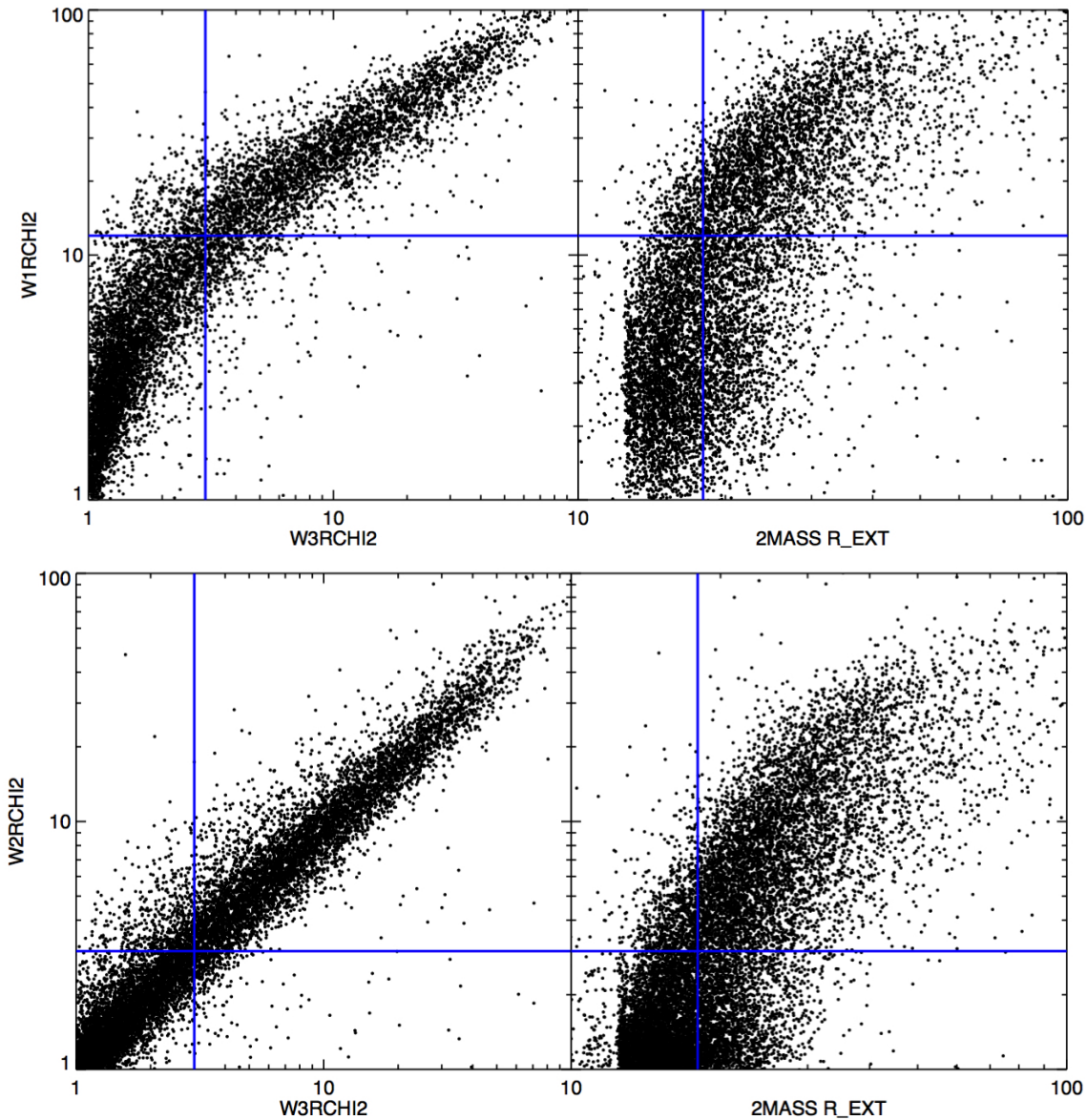


FIG. 24.— Correlations among size parameters for red extended sources in *WISE* with 2MASS Extended Source Catalog (XSC) counterparts. The y-axis in all plots corresponds to the RCHI2 parameter, which measures the goodness-of-fit of a source to a model for a point source (large values indicate a poor fit, so an extended source). The x-axis of the left panels is the RCHI2 parameter in the W3 band, (we used $W3RCHI2=3$, indicated by the vertical lines, to identify extended sources in our catalogs). The horizontal lines mark the approximate RCHI2 value in the W1 and W2 bands for typical red sources that meet this criterion. The x-axis of the right panels is the R_EXT parameter of the XSC, in units of arcseconds, describing the NIR angular size of the source. The vertical line shows the value of this parameter $18''$, that best corresponds to the W1 and W2 RCHI2 values typical of barely extended sources in W3. *Top*: correlations between the W1 RCHI2 parameter. *Bottom*: correlations with the W2 RCHI2 parameter.

1×10^5 galaxies. The only previous search for K3's in the refereed literature, that of Annis (1999), surveyed 163 galaxies.

As a check, we also used the R_EXT parameter in the XSC, which corresponds to a measure of the NIR angular size of these galaxies. The right hand panels in Figure 24 show that R_EXT corresponds to the angular sizes we are interested in with good sensitivity (i.e., the test $R_EXT > 18''$ has a low false negative rate), although it is not very specific (i.e. it has roughly a 50% false positive rate) for these red sources.

A query of the entire XSC with $|b| \geq 10$ and $R_EXT \geq 18$ yields 229,813 sources. A random sampling of 100 of these sources reveals that all are present in the WISE All-sky catalog, 45 have $W1RCHI2 > 12$ and 43 have $W2RCHI2 > 3$. These numbers are consistent with the specificity we estimated among the MIR-red sources in Figure 24. We also tested 100 random WISE sources satisfying our extended source criteria in W1 and W2, and find that 86 and 87 of them, respectively, have $R_EXT > 18''$, also consistent with the sensitivity suggested in Figure 24.

We conclude that there are $\sim 1 \times 10^5$ galaxies with sufficient angular size that they would have been included in our platinum sample if they had had significant W3 emission. In our survey of these $\sim 1 \times 10^5$ galaxies, we have found that there are no alien, non-stellar energy supplies in excess of 5.7 times the stellar luminosity of their host galaxy, and no alien supercivilizations reprocessing as much as 85% of their starlight into the MIR. We have found 50 galaxies consistent with 50% reprocessing, all of which are presumably extraordinary, but entirely natural, star-forming galaxies. Verification of the natural origin of the MIR flux in these 50 galaxies will thus lower our upper limit to 50%.

8. CONCLUSIONS

We have produced a clean catalog of the reddest extended sources in outside the Zone of Avoidance using in the WISE All-sky catalog, and corrected that catalog's photometry of extended sources to be consistent with careful aperture photometry at the 3-5% level. We used the point source goodness-of-fit parameter $W\#RCHI2$ to identify extended sources, and various tests (including visual inspection and interrogation of the Level 1b WISE data) to clean this sample of instrumental and data pipeline artifacts and point sources.

We have graded each of our sources in terms of its presence in the published literature, to determine whether the nature of its MIR emission is well understood.

Our motivation is to use this catalog to perform the first extragalactic search for waste heat from galaxy-spanning alien supercivilizations. To that end, we have used the AGENT formalism of Wright et al. (2014a) to interpret the WISE SEDs of these sources as ordinary elliptical galaxies with alien waste heat luminosities equal to a fraction γ of the starlight and characteristic temperature T_{waste} . This is an inappropriate model for natural sources, especially spirals and star-forming galaxies, but it provides a conservative upper limit on the true γ parameter for the galaxy.

We find that there are no galaxies in our sample of

1×10^5 galaxies with fit values of $\gamma > 0.85$, meaning that no galaxies resolved by WISE contain galaxy-spanning supercivilizations with energy supplies greater than 85% of the starlight in the galaxy (unless this energy is not primarily expelled as light in the WISE bandpasses). We have further identified all 50 resolved galaxies in our sample with fit values of $\gamma > 0.5$. More detailed SED modeling of these galaxies, including the use of other bands, will allow for more stringent upper limits, and we will perform such modeling in the future.

We also identify 93 sources with $\gamma > 0.25$ but very little study in the scientific literature. Three of these sources are MIR-bright and red galaxies that are essentially new to science, having little or no literature presence beyond bare mentions of a detection by IRAS or other surveys.

Verification that the MIR flux in all of these galaxies is predominantly from natural sources (e.g., through SED modeling across many more bands than WISE offers or spectroscopy) will push our upper limit on galaxy-spanning alien energy supplies in our sample of 1×10^5 galaxies down to 50% of the available starlight. In the meantime, these are the best candidates in the Local Universe for Type III Kardashev civilizations. This limit will improve upon the limit of $\alpha < 75\%$ found by Annis (1999) in 57 spiral and 106 elliptical galaxies.

We find that the Be shell star 48 Librae has a large extended MIR nebula. If the source of this dust is 48 Librae itself, it would suggest, surprisingly, that dwarf Be shell stars can be sites of significant dust production.

We have also found a previously unstudied cluster of MIR-bright sources with no optical counterparts and very red colors. They appear to be Galactic sources associated with a cloud, and so are likely part of a previously unstudied star forming region.

In the appendices, we have also illustrated how WISE can be used to rule out broad classes of K3 civilizations as being responsible for the lack of emission in so-called H I dark galaxies and the anomalous colors and morphologies of "red" (or "passive") spirals. We find a sample of five "red" spirals with red MIR and ($NUV - r$) colors, which are inconsistent with high levels of star formation but consistent with high levels of alien waste heat. Significant internal extinction would be a satisfactory natural explanation for these colors, but until that is ruled out these galaxies are some of the best candidates for K3's in our search to date.

This research is supported entirely by the John Templeton Foundation through its New Frontiers in Astronomy and Cosmology, administered by Don York of the University of Chicago. We are grateful for the opportunity provided by this grant to perform this research.

We thank Jason Young and Sharon X. Wang for discussions on the typical sizes and surface brightnesses of galaxies, especially LSBs. We thank Caryl Gronwall, and Lea Hagan for their assistance with NED. We thank Tom Jarrett for sharing a preliminary version of his extended source catalog. We thank the WISE team for making the WISE All-sky survey, and especially Davy Kirkpatrick for useful discussions and assistance navigating the WISE data products. We thank Richard Wade for

illuminating the nature of 48 Librae, and Leisa Townsley, Stan Owocki, Thomas Rivinius, Howard Bond, and Eric Fiegelson for discussions about the nature of dust around Be stars.

We thank Eric Mamajek for his inordinate efforts in hunting down photometry and kinematics for our strange no-optical-counterpart cluster and 48 Librae.

This publication makes use of data products from the Wide-field Infrared Survey Explorer, which is a joint project of the University of California, Los Angeles, and the Jet Propulsion Laboratory (JPL)/California Institute of Technology (Caltech), funded by the National Aeronautics and Space Administration (NASA). This work is based in part on observations made with the Spitzer Space Telescope, which is operated by JPL/Caltech under a contract with NASA. This research has made use of the NASA/IPAC Extragalactic Database (NED) which is operated by JPL/Caltech, under contract with NASA.

The Digitized Sky Surveys were produced at the Space Telescope Science Institute under U.S. Government grant NAG W-2166. The images of these surveys are based on photographic data obtained using the Oschin Schmidt Telescope on Palomar Mountain and the UK Schmidt Telescope. The plates were processed into the present compressed digital form with the permission of these institutions. The Second Palomar Observatory Sky Survey (POSS-II) was made by the California Institute of Technology with funds from the National Science Foundation,

the National Geographic Society, the Sloan Foundation, the Samuel Oschin Foundation, and the Eastman Kodak Corporation.

Funding for the Sloan Digital Sky Survey (SDSS) has been provided by the Alfred P. Sloan Foundation, the Participating Institutions, NASA, the National Science Foundation, the U.S. Department of Energy, the Japanese Monbukagakusho, and the Max Planck Society. The SDSS Web site is <http://www.sdss.org/>.

The SDSS is managed by the Astrophysical Research Consortium (ARC) for the Participating Institutions. The Participating Institutions are The University of Chicago, Fermilab, the Institute for Advanced Study, the Japan Participation Group, The Johns Hopkins University, Los Alamos National Laboratory, the Max-Planck-Institute for Astronomy (MPIA), the Max-Planck-Institute for Astrophysics (MPA), New Mexico State University, University of Pittsburgh, Princeton University, the United States Naval Observatory, and the University of Washington.

Based on observations made with the NASA Galaxy Evolution Explorer. GALEX is operated for NASA by the California Institute of Technology under NASA contract NAS5-98034.

The Center for Exoplanets and Habitable Worlds is supported by the Pennsylvania State University, the Eberly College of Science, and the Pennsylvania Space Grant Consortium.

APPENDIX

H I DARK GALAXIES

So-called “dark galaxies” are galaxies with no detectable stellar component (i.e. composed entirely of dark matter, and perhaps gas). The HIPASS (e.g. Wong et al. 2006) and ALFALFA (Giovanelli et al. 2007) surveys of H I are sensitive to neutral hydrogen in galaxies, and those detections with little no detectable optical emission are candidate “dark galaxies” or “almost dark galaxies” (Martinkus et al. 2014).

Such galaxies are consistent with $\alpha \sim 1$ — that is, galaxies in which all or nearly all of the starlight is absorbed to power a galaxy-wide civilization, or K3. If $\gamma \sim \alpha$ (i.e. the energy were all radiated as waste heat) and $T_{\text{waste}} \gtrsim 150$ K, such a galaxy would be very bright in the MIR, and the \hat{G} survey would find them easily.

As a check, and to ensure that we include even those known H I galaxies that might not be resolved by *WISE*, we have examined the ALFALFA and NOIRCAT (Northern HIPASS Optical/IR Catalog) survey galaxies using *WISE* imaging.

To within $5''$, only 67 of the 730 sources in the ALFALFA sample and 78 of the 1002 sources from the NOIRCAT (northern HIPASS) sample matched to a *WISE* source. We constructed “at-a-glance” charts for all 1732 sources from the two surveys. In no case is there a bright MIR source coincident with the H I and little or no optical emission.¹² It is safe to say that these dark galaxies are probably not examples of K3s.

We note that a similar analysis was performed by Pérez et al. (2014), though probably for a different purpose.

PASSIVE SPIRALS

One possible application of energy for a galaxy-spanning civilization might be to alter the underlying stellar population in some way, for instance suppressing high-mass star formation to prevent supernova explosions. Such a galaxy might appear morphologically similar to a spiral, but lack supernova progenitors and other signatures of high mass star formation. This is consistent with “passive spirals” or “red spirals” (see Masters et al. 2010, and references therein), and so we explore here if such galaxies are anomalously bright in the MIR.

Cortese (2012) argued that optically selected “red spirals” are not, in fact, passive, but simply have old populations in addition to active current star formation. That is, in very high mass systems ($> 10^{10} M_{\odot}$) optical colors are more sensitive to star formation history than to the instantaneous star formation rate. Cortese argued that $NUV - r$ colors were a better proxy for activity/quiescence than optical colors, and showed that “red spirals” typically have

¹² We point out that at least one object in Platinum sample (entry 50 in Table 9, HIPASS J1403-50) is a HIPASS galaxy, and

was given a grade of B. This object is not, however, optically faint.

$(NUV - r) < 4$, consistent with star formation rates typical of ordinary spirals. Cortese selected only face-on spirals to minimize the effects of extinction in the NUV (which would ruin this band’s diagnostic power).

It follows, then that a “red spiral” with an anomalously red ($NUV - r$) color might be a truly passive spiral, which would make a high MIR flux anomalous.

We investigated the sample of red spiral galaxies presented in Masters et al. (2010). We matched their list of 5433 sources to *WISE* using a $3''$ search radius and recovered *WISE* photometry for $\sim 99.5\%$ of the sample. We recover *WISE* photometry for 27 more sources by opening up the search radius to $20''$. For our NUV photometry we matched this list to GALEX and recovered photometry for $\sim 88\%$ of the sources. All of these Galaxy Zoo galaxies have good r -band photometry from the Sloan Digital Sky Survey.

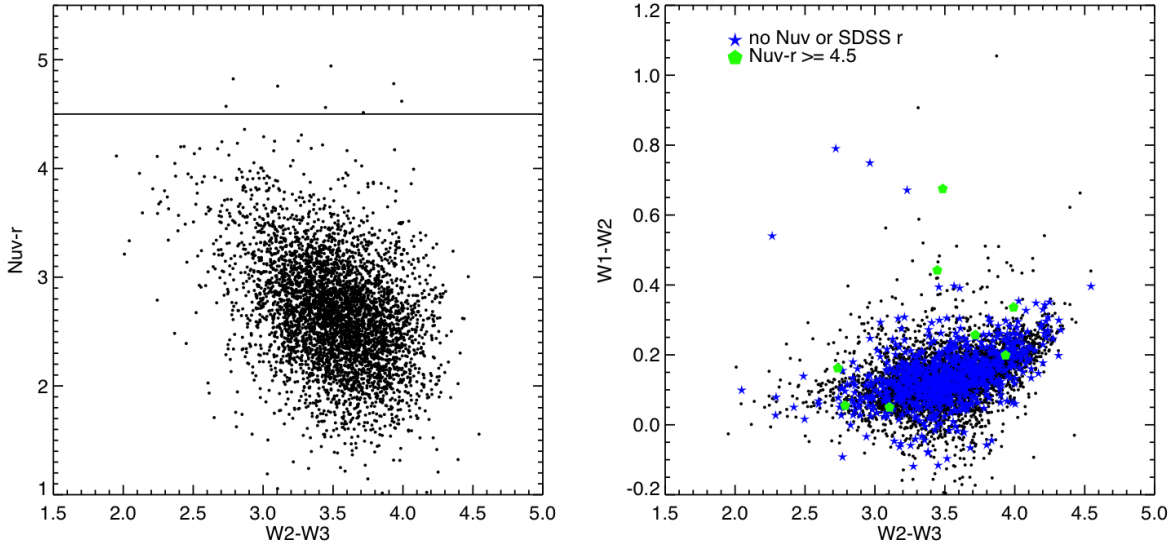


FIG. 25.— (Left) We plot GALEX $NUV-r$ versus $W2-W3$ for a large sample of red spiral galaxies. The solid horizontal line represents $NUV-r \geq 4.5$. (Right) We plot $W1-W2$ versus $W2-W3$ for approximately 100% of the red spiral galaxy sample. Green points indicate the extreme $NUV-r$ sources, while the blue points represent sources which could not be included in the left hand plot due to the lack of photometric measurement.

The left panel of Figure 25 shows $NUV - r$ colors for our sample. In agreement with Cortese we find that most red spirals have $(NUV - r) < 4$, with some scattering to higher values (consistent with some having extreme extinction). Eight galaxies in our sample have $(NUV - r) > 4.5$ which would put them firmly in the “red sequence” of passive galaxies, if they were unextinguished.

The right panel of Figure 25 shows a *WISE* color-color plot of the entire sample (irrespective of the availability of GALEX NUV data), with the anomalously red galaxies highlighted. Five of these sources have moderately red ($W2 - W3$) colors, consistent with high rates of star formation. Either these five galaxies suffer from significant extinction, or they are examples of anomalous MIR-bright, passive spiral galaxies, perhaps consistent with a K3. Visual examination reveals that none are edge-on; all are at modest inclination.

We list these five potentially anomalous sources with their AGENT parameters in Table 5.

TABLE 5
 FIVE SPIRALS RED IN OPTICAL, $NUV - r$, AND MIR COLORS

<i>WISE</i> designation	$(NUV - r)$	T_{waste}	γ	SIMBAD name
J085428.94+084444.4	4.62	179	0.258	2MASX J08542894+08444430
J113325.93+141618.9	4.94	180	0.198	2MASX J11332590+1416186
J142619.17+473357.8	4.51	180	0.202	SDSS J142619.17+473357.7
J142859.55+605000.5	4.56	163	0.212	2MASX J14285959+6050005
J230616.43+135856.4	4.78	239	0.172	2MASXJ23061640+1358560

REFERENCES

- Adams, J. J., Simon, J. D., Bolatto, A. D., et al. 2013, *ApJ*, 771, 112 [6.3.5](#)
- Annis, J. 1999, *Journal of the British Interplanetary Society*, 52, 19 [1.2](#), [7.2](#), [8](#)
- Bridge, C. R., Blain, A., Borys, C. J. K., et al. 2013, *ApJ*, 769, 91 [6.3.1](#)
- Carballo, R., Wesseliuss, P. R., & Whittet, D. C. B. 1992, *A&A*, 262, 106 [6.3.5](#)
- Carrigan, Jr., R. A. 2009a, *ApJ*, 698, 2075 [1.2](#)
- Carrigan, Jr., R. A. 2009b, in *Astronomical Society of the Pacific Conference Series*, Vol. 420, *Bioastronomy 2007: Molecules, Microbes and Extraterrestrial Life*, ed. K. J. Meech, J. V. Keane, M. J. Mumma, J. L. Siefert, & D. J. Werthimer, 415 [1.2](#)
- , 2012, *Acta Astronautica*, 78, 121 [1.2](#)
- Chen, R., Peng, B., Strom, R. G., & Wei, J. 2011, *MNRAS*, 412, 2433 [6.3.3](#)
- Condon, J. J., Cotton, W. D., Greisen, E. W., et al. 1998, *AJ*, 115, 1693 [6.3.1](#), [6.3.2](#)
- Cortese, L. 2012, *A&A*, 543, A132 [B](#), [B](#)
- Cotton, W. D., Condon, J. J., & Arbizzani, E. 1999, *ApJS*, 125, 409 [3](#)
- Dey, A., Soifer, B. T., Desai, V., et al. 2008, *ApJ*, 677, 943 [6.3.1](#)
- Dyson, F. J. 1960, *Science*, 131, 1667 [1.2](#)
- Edelson, R., & Malkan, M. 2012, *ApJ*, 751, 52 [6.3.1](#)
- Eisenhardt, P. R. M., Wu, J., Tsai, C.-W., et al. 2012, *ApJ*, 755, 173 [6.3.1](#)
- Everett, J. E., & Churchwell, E. 2010, *ApJ*, 713, 592 [6.3.5](#)
- Falco, E. E., Kurtz, M. J., Geller, M. J., et al. 1999, *PASP*, 111, 438 [3](#)
- Giovanelli, R., Haynes, M. P., Kent, B. R., et al. 2007, *AJ*, 133, 2569 [A](#)
- Gontcharov, G. A. 2006, *Astronomy Letters*, 32, 759 [6.3.5](#)
- Hart, M. H. 1975, *QJRAS*, 16, 128 [1.1](#)
- Hoaglin, D. C., Mosteller, F., & Tukey, J. W. 1983, *Wiley Series in Probability and Mathematical Statistics*, New York: Wiley, 1983, edited by Hoaglin, David C.; Mosteller, Frederick; Tukey, John W., [9](#)
- Hoffleit, D., & Warren, Jr., W. H. 1995, *VizieR Online Data Catalog*, 5050, 0 [6.3.5](#)
- Hwang, H. S., & Geller, M. J. 2013, *ApJ*, 769, 116 [6.3.1](#)
- Jarrett, T. H., Masci, F., Tsai, C. W., et al. 2012, *AJ*, 144, 68 [2.2](#)
- Jarrett, T. H., Masci, F., Tsai, C. W., et al. 2013, *AJ*, 145, 6 [2.2](#)
- Jaschek, C., & Jaschek, M. 1992, *A&AS*, 95, 535 [6.3.5](#)
- Jugaku, J., & Nishimura, S. 1991, in *Lecture Notes in Physics*, Berlin Springer Verlag, Vol. 390, *Bioastronomy: The Search for Extraterrestrial Life — The Exploration Broadens*, ed. J. Heidmann & M. J. Klein, 295–298 [1.2](#)
- Jugaku, J., & Nishimura, S. 1997, in *IAU Colloq.* 161: *Astronomical and Biochemical Origins and the Search for Life in the Universe*, ed. C. Batalli Cosmovici, S. Bowyer, & D. Werthimer, 707 [1.2](#)
- Jugaku, J., & Nishimura, S. 2000, in *Astronomical Society of the Pacific Conference Series*, Vol. 213, *Bioastronomy 99*, ed. G. Lemarchand & K. Meech, 581 [1.2](#)
- Jugaku, J., & Nishimura, S. 2004, in *IAU Symposium*, Vol. 213, *Bioastronomy 2002: Life Among the Stars*, ed. R. Norris & F. Stootman, 437 [1.2](#)
- Jugaku, J., Noguchi, K., & Nishimura, S. 1995, in *Astronomical Society of the Pacific Conference Series*, Vol. 74, *Progress in the Search for Extraterrestrial Life*, ed. G. S. Shostak, 381 [1.2](#)
- Kalas, P., Graham, J. R., Beckwith, S. V. W., Jewitt, D. C., & Lloyd, J. P. 2002, *ApJ*, 567, 999 [6.3.5](#)
- Kardashev, N. S. 1964, *Soviet Ast.*, 8, 217 [1.1](#)
- Lauberts, A., & Valentijn, E. A. 1988, in *European Southern Observatory Conference and Workshop Proceedings*, Vol. 28, *European Southern Observatory Conference and Workshop Proceedings*, ed. F. Murtagh, A. Heck, & P. Benvenuti, 37–42 [3](#)
- Lavaux, G., & Hudson, M. J. 2011, *MNRAS*, 416, 2840 [3](#)
- Lawrence, A., Rowan-Robinson, M., Ellis, R. S., et al. 1999, *MNRAS*, 308, 897 [3](#)
- Lee, C.-D., Chen, W.-P., & Kinoshita, D. 2011, in *IAU Symposium*, Vol. 272, *IAU Symposium*, ed. C. Neiner, G. Wade, G. Meynet, & G. Peters, 404–405 [6.3.5](#)
- Martinkus, C., Cannon, J. M., Adams, E. A., et al. 2014, in *American Astronomical Society Meeting Abstracts*, Vol. 223, *American Astronomical Society Meeting Abstracts #223*, 246.51 [A](#)
- Masters, K. L., Mosleh, M., Romer, A. K., et al. 2010, *MNRAS*, 405, 783 [B](#)
- Meyer, M. R., Hillenbrand, L. A., Backman, D., et al. 2006, *PASP*, 118, 1690 [6.3.1](#)
- Mihalas, D., & Binney, J. 1981, San Francisco, CA, W. H. Freeman and Co., 1981. 608 p., [6.3.5](#)
- Miroshnichenko, A. S., & Bjorkman, K. S. 2000, in *Astronomical Society of the Pacific Conference Series*, Vol. 214, *IAU Colloq.* 175: *The Be Phenomenon in Early-Type Stars*, ed. M. A. Smith, H. F. Henrichs, & J. Fabregat, 484 [6.3.5](#)
- Miroshnichenko, A. S., Levato, H., Bjorkman, K. S., & Grosso, M. 2001, *A&A*, 371, 600 [6.3.5](#)
- Mitronova, S. N., Karachentsev, I. D., Karachentseva, V. E., Jarrett, T. H., & Kudrya, Y. N. 2004, *Bulletin of the Special Astrophysics 1 Observatory*, 57, 5 [3](#)
- Moshir, M. et al. 1992, *Explanatory Supplement to the IRAS Faint Source Survey*, version 2, JPL D-10015 8/92 (Pasadena: JPL). [6.3.2](#)
- Paturel, G., Petit, C., Garnier, R., & Prugniel, P. 2000, *A&AS*, 144, 475 [3](#)
- Pérez, J., Arrieta, A., Pantoja, C., et al. 2014, in *American Astronomical Society Meeting Abstracts*, Vol. 223, *American Astronomical Society Meeting Abstracts #223*, 246.50 [A](#)
- Povich, M. S., Benjamin, R. A., Whitney, B. A., et al. 2008, *ApJ*, 689, 242 [6.3.5](#)
- Ramella, M., Geller, M. J., Pisani, A., & da Costa, L. N. 2002, *AJ*, 123, 2976 [3](#)
- Rivinius, T., Carciofi, A. C., & Martayan, C. 2013, *A&A Rev.*, 21, 69 [6.3.5](#)
- Saunders, W., Sutherland, W. J., Maddox, S. J., et al. 2000, *MNRAS*, 317, 55 [3](#)
- Silva, L., Granato, G. L., Bressan, A., & Danese, L. 1998, *ApJ*, 509, 103 [4.1](#)
- Slysh, V. I. 1985, in *IAU Symposium*, Vol. 112, *The Search for Extraterrestrial Life: Recent Developments*, ed. M. D. Papagiannis, 315–319 [1.2](#)
- Stern, D., Lansbury, G. B., Assef, R. J., et al. 2014, arXiv:1403.3078, arXiv:1403.3078 [6.3.1](#)
- Strauss, M. A., Huchra, J. P., Davis, M., et al. 1992, *ApJS*, 83, 29 [6.3.1](#)
- Takase, B., & Miyauchi-Isobe, N. 1984, *Annals of the Tokyo Astronomical Observatory*, 19, 595 [3](#)
- Štefl, S., Le Bouquin, J.-B., Carciofi, A. C., et al. 2012, *A&A*, 540, A76 [6.3.5](#)
- van Buren, D., & McCray, R. 1988, *ApJ*, 329, L93 [6.3.5](#)
- van Leeuwen, F. 2009, *A&A*, 497, 209 [6.3.1](#), [6.3.5](#), [6.3.5](#)
- Voges, W., Aschenbach, B., Boller, T., et al. 1999, *A&A*, 349, 389 [6.3.1](#)
- Wang, L., & Rowan-Robinson, M. 2009, *MNRAS*, 398, 109 [3](#)
- Wong, O. I., Ryan-Weber, E. V., Garcia-Appadoo, D. A., et al. 2006, *MNRAS*, 371, 1855 [A](#)
- Wright, E. L., Eisenhardt, P. R. M., Mainzer, A. K., et al. 2010, *AJ*, 140, 1868 [1.2](#), [2](#)
- Wright, J. T., Griffith, R. L., Sigurdsson, S., Povich, M. S., & Mullan, B. 2014a, *The Astrophysical Journal*, 792, 27 [1](#), [1.3](#), [4.1](#), [6.2](#), [7.1](#), [8](#)
- Wright, J. T., Mullan, B., Sigurdsson, S., & Povich, M. S. 2014b, *The Astrophysical Journal*, 792, 26 [1](#)
- Wu, J., Tsai, C.-W., Sayers, J., et al. 2012, *ApJ*, 756, 96 [6.3.1](#)
- Wu, Y.-Z., Zhao, Y.-H., & Meng, X.-M. 2011, *ApJS*, 195, 17 [6.2](#)
- Yang, J., Jiang, Z., Wang, M., Ju, B., & Wang, H. 2002, *ApJS*, 141, 157 [6.3.1](#), [10](#)

TABLE 6
EXTREME WISE COLORS

RA hhmmss.ss	DEC ddmms.s	SIMBAD type	Grade	W1 mag.	W2 mag.	W3 mag.	W4 mag.	Color mag.	γ	T_{waste} K	Photometry	Note
W1-W2 Most Extreme Sources												
072533.95	+292919.9	PN	C	11.20	8.89	4.33	0.44	2.31	0.83	123	2	NGC 2371
213652.95	+124719.2	PN	C	11.68	9.49	5.25	0.53	2.19	0.92	98	2	NGC 7094
180600.64	+002235.5	PN	C	15.12	13.01	8.52	3.56	2.11	0.90	248	1	PN-G028.0+
054206.16	+090511.6	PN	C	10.06	7.98	4.07	-0.33	2.09	0.83	106	2	NGC 2022
060253.97	-710310.0	LIN	C	11.59	9.52	6.14	3.25	2.07	0.66	349	0	2MASX J06025406
122430.65	-184700.7	PN	C	9.61	7.66	4.33	0.00	1.95	0.71	108	2	NGC 4361
214035.92	+663525.8	Y*O	B	10.05	8.25	5.58	3.05	1.80	0.45	403	1	2MASS J21403852
194357.75	-140913.5	PN	C	8.85	7.09	3.14	-0.88	1.75	0.72	118	2	NGC 6818
193121.41	-723921.3	Sy2	C	10.29	8.54	5.55	2.06	1.75	0.36	137	2	Antennae
003443.48	-000226.6	Sy2	C	11.72	9.98	6.57	3.84	1.74	0.54	347	2	2MFGC-40
W2-W3 Most Extreme Sources												
091742.98	+131214.8	Comet	C	12.76	11.50	5.02	0.99	6.49	0.93	204	2	29P/Schwassmann-Wachm
155812.25	-141806.2	IR	B	16.48	15.39	9.13	4.03	6.26	0.99	89	0	IRAS-15553-1
235821.58	-320748.6	Comet	C	16.56	15.71	9.92	4.97	5.79	0.97	93	1	Garradd 2009
045608.93	-674947.5		C	14.39	14.51	8.79	6.52	5.71	0.51	211	1	Object in LM
122654.61	-005239.1	Sy2	C	10.04	9.15	3.81	-0.15	5.34	0.85	120	2	NGC 4355
052703.47	-664959.2		C	15.10	14.63	9.32	7.90	5.31	0.45	282	0	Object in LM
100918.85	-805128.1	PN	C	10.81	9.80	4.61	2.88	5.19	0.59	290	2	NGC 3195
055542.61	+032331.8	H2G	C	10.99	10.12	4.94	1.52	5.18	0.72	142	2	UGCA 110
061452.97	-062244.4	Y*O	B	8.80	8.31	3.15	1.78	5.16	0.42	289	2	IRAS 06124-0
004036.06	+410117.9	HII	C	14.43	13.76	8.62	6.45	5.13	0.52	263	0	BA1-441
W1-W3 Most Extreme Sources												
091742.98	+131214.8	Comet	C	12.76	11.50	5.02	0.99	7.74	0.93	204	2	29P/Schwassmann-Wachm
155812.25	-141806.2	IR	B	16.48	15.39	9.13	4.03	7.34	0.99	89	0	IRAS-15553-1
072533.95	+292919.9	PN	C	11.20	8.89	4.33	0.44	6.87	0.83	123	2	NGC 2371
235821.58	-320748.6	Comet	C	16.56	15.71	9.92	4.97	6.64	0.97	93	1	Garradd 2009
180600.64	+002235.5	PN	C	15.12	13.01	8.52	3.56	6.60	0.90	248	1	PN-G028.0+
213652.95	+124719.2	PN	C	11.68	9.49	5.25	0.53	6.43	0.92	98	2	NGC 7094
190101.24	-181215.0	PN	C	15.50	13.89	9.08	3.07	6.42	0.99	73	1	PN A6651
185334.98	+330152.2	PN	C	11.79	10.33	5.48	0.85	6.30	0.93	100	1	Ring Nebul
122654.61	-005239.1	Sy2	C	10.04	9.15	3.81	-0.15	6.23	0.85	120	2	NGC 4355
041415.79	-124420.7	PN	C	9.12	7.98	2.91	-0.05	6.21	0.69	258	2	NGC 1535
W3-W4 Most Extreme Sources												
190101.24	-181215.0	PN	C	15.50	13.89	9.08	3.07	6.01	0.99	73	1	PNA6651
095551.65	+694046.6	Em*	C	6.38	5.40	3.73	-1.79	5.53	0.75	77	1	[DOB2000]-
032910.31	+312158.0	Y*O	C	6.76	5.85	3.62	-1.63	5.25	0.73	83	1	[LAL96]-21
155812.25	-141806.2	IR	B	16.48	15.39	9.13	4.03	5.10	0.99	89	0	IRAS-15553-1
215935.03	-392308.7	PN	C	16.42	15.54	10.75	5.70	5.05	0.95	90	1	IC 5148
180600.64	+002235.5	PN	C	15.12	13.01	8.52	3.56	4.96	0.90	248	1	PN-G028.0+
235821.58	-320748.6	Comet	C	16.56	15.71	9.92	4.97	4.94	0.97	93	1	Garradd 2009
071448.80	-465733.6	PN	C	11.68	10.09	6.39	1.59	4.79	0.86	95	2	ESO 256-1
213652.95	+124719.2	PN	C	11.68	9.49	5.25	0.53	4.72	0.92	98	2	NGC 7094
160426.50	+404059.1	PN	C	12.54	12.04	7.48	2.78	4.70	0.87	98	2	NGC 6058
W1-W4 Most Extreme Sources												
155812.25	-141806.2	IR	B	16.48	15.39	9.13	4.03	12.45	0.99	89	0	IRAS-15553-1
190101.24	-181215.0	PN	C	15.50	13.89	9.08	3.07	12.43	0.99	73	1	PN A6651
091742.98	+131214.8	Comet	C	12.76	11.50	5.02	0.99	11.77	0.93	204	2	29P/Schwassmann-Wachm
235821.58	-320748.6	Comet	C	16.56	15.71	9.92	4.97	11.58	0.97	93	1	Garradd 2009
180600.64	+002235.5	PN	C	15.12	13.01	8.52	3.56	11.56	0.90	248	1	PN-G028.0+
213652.95	+124719.2	PN	C	11.68	9.49	5.25	0.53	11.15	0.92	98	2	NGC 7094
185334.98	+330152.2	PN	C	11.79	10.33	5.48	0.85	10.94	0.93	100	1	Ring Nebul
072533.95	+292919.9	PN	C	11.20	8.89	4.33	0.44	10.76	0.83	123	2	NGC 2371
215935.03	-392308.7	PN	C	16.42	15.54	10.75	5.70	10.71	0.95	90	1	IC 5148
160628.19	-354520.9	PN	C	10.61	9.25	4.52	0.08	10.53	0.89	105	2	PN-G341.5+
W2-W4 Most Extreme Sources												
155812.25	-141806.2	IR	B	16.48	15.39	9.13	4.03	11.36	0.99	89	0	IRAS-15553-1
190101.24	-181215.0	PN	C	15.50	13.89	9.08	3.07	10.82	0.99	73	1	PN A6651
235821.58	-320748.6	Comet	C	16.56	15.71	9.92	4.97	10.73	0.97	93	1	Garradd 2009
091742.98	+131214.8	Comet	C	12.76	11.50	5.02	0.99	10.52	0.93	204	2	29P/Schwassmann-Wachm
215935.03	-392308.7	PN	C	16.42	15.54	10.75	5.70	9.83	0.95	90	1	IC 5148
185334.98	+330152.2	PN	C	11.79	10.33	5.48	0.85	9.48	0.93	100	1	Ring Nebul

TABLE 6 — *Continued*

RA hhmmss.ss	DEC ddmmss.s	SIMBAD type	Grade	W1 mag.	W2 mag.	W3 mag.	W4 mag.	Color mag.	γ	T_{waste} K	Photometry	Note
180600.64	+002235.5	PN	C	15.12	13.01	8.52	3.56	9.45	0.90	248	1	PN-G028.0+10.2
122654.61	-005239.1	Sy2	C	10.04	9.15	3.81	-0.15	9.30	0.85	120	2	NGC 4355
160426.50	+404059.1	PN	C	12.54	12.04	7.48	2.78	9.25	0.87	98	2	NGC 6058
160628.19	-354520.9	PN	C	10.61	9.25	4.52	0.08	9.17	0.89	105	2	PN-G341.5+12.1

TABLE 7
GALAXIES WITH EXTREME WISE COLORS

RA hhmmss.ss	DEC ddmmss.s	SIMBAD type	Grade ¹	W1 mag.	W2 mag.	W3 mag.	W4 mag.	Color mag.	γ	T_{waste} K	Photometry ²	Note
W1-W2 Most Extreme Galaxies												
060253.97	-710310.0	LIN	C	11.59	9.52	6.14	3.25	2.07	0.66	349	0	2MASX J06025406-710
193121.41	-723921.3	Sy2	C	10.29	8.54	5.55	2.06	1.75	0.36	137	2	SUPER ANTENNA
003443.48	-000226.6	Sy2	C	11.72	9.98	6.57	3.84	1.74	0.54	347	2	2MFGC-403
080106.63	-660914.9	G	C	10.20	8.51	5.24	2.17	1.69	0.52	338	2	6dFGSg J080106.6-660
002153.60	-791007.8	Sy2	C	10.06	8.39	5.22	2.14	1.67	0.49	341	2	2MASX J00215355-791
100125.94	+154612.2	G	C	7.99	6.33	4.06	1.14	1.65	0.34	401	2	NGC 3094
033639.05	-205406.8	GiG	C	9.58	7.98	4.69	1.50	1.60	0.50	328	2	NGC 1377
183820.32	-652539.0	Sy2	C	9.37	7.80	4.32	1.21	1.57	0.52	322	2	ESO 103-35
173801.51	+561325.9	Sy2	C	11.08	9.57	6.19	3.51	1.51	0.45	343	2	2MASX J17380143+561
112402.72	-282315.4	Sy2	C	10.81	9.31	5.98	3.60	1.50	0.43	359	2	IRAS 11215-2806
W2-W3 Most Extreme Galaxies												
122654.61	-005239.1	Sy2	C	10.04	9.15	3.81	-0.15	5.34	0.85	120	2	NGC 4355
055542.61	+032331.8	H2G	C	10.99	10.12	4.94	1.52	5.18	0.72	142	2	UGCA 116
042826.03	-043349.2	LIN	C	11.62	10.99	5.92	2.00	5.06	0.79	121	2	IRAS 04259-0440
103833.62	-071014.4	G	C	9.49	9.10	4.14	0.80	4.97	0.61	146	1	IC 630
001850.88	-102236.6	EmG	C	10.76	10.29	5.41	2.37	4.89	0.52	162	0	MCG 02-01-051
181338.76	-574356.9	G	C	11.26	10.84	5.99	2.57	4.85	0.60	142	0	IC 4686
225234.71	+244349.4	AGN	C	11.44	10.87	6.06	2.67	4.81	0.60	143	2	Mrk 309
010426.95	-640712.2	H2G	C	11.23	10.81	6.03	2.78	4.78	0.54	150	0	ESO 79-16
195405.20	+495647.0	G	B	12.57	12.16	7.39	4.81	4.76	0.39	195	0	LEDA 200363
043400.03	-083444.9	AGN	C	8.74	8.21	3.54	-0.07	4.67	0.63	133	2	NGC 1614
W1-W3 Most Extreme Galaxies												
122654.61	-005239.1	Sy2	C	10.04	9.15	3.81	-0.15	6.23	0.85	120	2	NGC 4355
055542.61	+032331.8	H2G	C	10.99	10.12	4.94	1.52	6.06	0.72	142	2	UGCA 116
205826.80	-423900.3	LIN	C	11.08	9.69	5.33	1.75	5.75	0.65	135	2	ESO 286-19
042826.03	-043349.2	LIN	C	11.62	10.99	5.92	2.00	5.69	0.79	121	2	IRAS 04259-0440
003652.44	-333316.8	AGN	C	10.52	9.09	4.84	1.17	5.69	0.66	131	2	ESO 350-38
124930.16	-112403.4	Sy2	C	11.46	10.10	5.90	2.79	5.55	0.59	286	1	IRAS 12468-1107
060253.97	-710310.0	LIN	C	11.59	9.52	6.14	3.25	5.45	0.66	349	0	2MASX J06025406-710
012002.63	+142142.5	LIN	C	10.84	9.67	5.41	2.24	5.42	0.49	154	0	MCG+02-04-025
011607.20	+330521.7	Sy2	C	11.09	9.78	5.70	2.57	5.38	0.54	286	0	NGC 449
225234.71	+244349.4	AGN	C	11.44	10.87	6.06	2.67	5.38	0.60	143	2	Mrk 309
W3-W4 Most Extreme Galaxies												
131503.51	+243707.8	Q?	C	10.44	10.32	7.05	2.45	4.60	0.61	99	2	IC 860
153457.25	+233011.5	SyG	C	9.52	8.96	4.55	0.19	4.35	0.79	107	2	Arp 220
125145.54	+254628.5	IG	C	9.74	9.58	6.24	1.92	4.32	0.53	107	2	NGC 4747
000820.57	+403755.9	Sy2	C	12.41	12.27	8.58	4.44	4.14	0.54	113	3	2MASX J00082041+403
042759.96	-475445.8	LIN	C	9.52	9.44	6.79	2.81	3.98	0.27	115	2	CARAFE NEBULA
122654.61	-005239.1	Sy2	C	10.04	9.15	3.81	-0.15	3.96	0.85	120	2	NGC 4355
065558.96	-404912.2	G	B	11.12	10.72	7.34	3.41	3.93	0.43	119	2	6dFGSg J065559.0-404
042826.03	-043349.2	LIN	C	11.62	10.99	5.92	2.00	3.92	0.79	121	2	IRAS 04259-0440
102508.18	+170914.1	IG	C	12.56	12.15	8.06	4.15	3.92	0.58	121	0	NGC 3239
202825.49	-330420.5	G	B	10.33	10.32	7.15	3.29	3.86	0.32	121	2	ESO 400-28
W1-W4 Most Extreme Galaxies												
122654.61	-005239.1	Sy2	C	10.04	9.15	3.81	-0.15	10.19	0.85	120	2	NGC 4355
042826.03	-043349.2	LIN	C	11.62	10.99	5.92	2.00	9.61	0.79	121	2	IRAS 04259-0440
055542.61	+032331.8	H2G	C	10.99	10.12	4.94	1.52	9.47	0.72	142	2	UGCA 116
003652.44	-333316.8	AGN	C	10.52	9.09	4.84	1.17	9.35	0.66	131	2	ESO 350-38
153457.25	+233011.5	SyG	C	9.52	8.96	4.55	0.19	9.33	0.79	107	2	Arp 220
205826.80	-423900.3	LIN	C	11.08	9.69	5.33	1.75	9.33	0.65	135	2	ESO 286-19
205724.32	+170738.5	G	C	10.57	9.88	5.27	1.43	9.15	0.70	124	2	IRAS F20550+1655-
133955.96	-313824.4	AGN	C	8.27	7.00	2.95	-0.73	9.01	0.60	130	2	NGC 5253
150029.00	-262649.2	H2G	C	11.96	11.36	6.82	3.08	8.88	0.65	128	2	2MASX J15002897-262
231546.75	-590314.5	Sy2	C	10.69	9.67	5.34	1.87	8.83	0.57	139	2	ESO 148-2
W2-W4 Most Extreme Galaxies												
122654.61	-005239.1	Sy2	C	10.04	9.15	3.81	-0.15	9.30	0.85	120	2	NGC 4355
042826.03	-043349.2	LIN	C	11.62	10.99	5.92	2.00	8.98	0.79	121	2	IRAS 04259-0440
153457.25	+233011.5	SyG	C	9.52	8.96	4.55	0.19	8.77	0.79	107	2	Arp 220
055542.61	+032331.8	H2G	C	10.99	10.12	4.94	1.52	8.60	0.72	142	2	UGCA 116
205724.32	+170738.5	G	C	10.57	9.88	5.27	1.43	8.45	0.70	124	2	IRAS F20550+1655-
234709.20	+153548.3	Sy2	C	11.02	10.56	5.91	2.20	8.36	0.65	129	2	MCG+02-60-017

TABLE 7 — *Continued*

RA hhmmss.ss	DEC ddmmss.s	SIMBAD type	Grade ¹	W1 mag.	W2 mag.	W3 mag.	W4 mag.	Color mag.	γ	T_{waste} K	Photometry ²	Note
103833.62	-071014.4	G	C	9.49	9.10	4.14	0.80	8.31	0.61	146	1	IC 630
150029.00	-262649.2	H2G	C	11.96	11.36	6.82	3.08	8.29	0.65	128	2	2MASX J15002897-2626487
043400.03	-083444.9	AGN	C	8.74	8.21	3.54	-0.07	8.28	0.63	133	2	NGC 1614
181338.76	-574356.9	G	C	11.26	10.84	5.99	2.57	8.27	0.60	142	0	IC 4686

¹ *Grade* refers to how well understood an object is (see Section 4.3.) All of these objects have grade C indicating that they are understood, having been discussed in the refereed literature.

² *Photometry* refers to the source of the photometry used in the table: 0:Profile fit; 1:Aperture-corrected; 2:Calibrated, 3:Elliptical aperture. See Section 5.1

TABLE 8
GALAXIES WITH EXTREME *WISE* γ VALUES

RA hhmmss.ss	DEC ddmms.s	SIMBAD type	Grade ¹	W1 mag.	W2 mag.	W3 mag.	W4 mag.	γ	T_{waste} K	Photometry ²	Note
122654.61	-005239.1	Sy2	C	10.04	9.15	3.81	-0.15	0.85	120	2	NGC 4355
042826.03	-043349.2	LIN	C	11.62	10.99	5.92	2.00	0.79	121	2	IRAS 04259-0440
153457.25	+233011.5	SyG	C	9.52	8.96	4.55	0.19	0.79	107	2	Arp 220
055542.61	+032331.8	H2G	C	10.99	10.12	4.94	1.52	0.72	142	2	UGCA 116
205724.32	+170738.5	G	C	10.57	9.88	5.27	1.43	0.70	124	2	IRAS F20550+1655-SE
060253.97	-710310.0	LIN	C	11.59	9.52	6.14	3.25	0.66	349	0	2MASX J06025406-7103104
003652.44	-333316.8	AGN	C	10.52	9.09	4.84	1.17	0.66	131	2	ESO 350-38
150029.00	-262649.2	H2G	C	11.96	11.36	6.82	3.08	0.65	128	2	2MASX J15002897-2626487
234709.20	+153548.3	Sy2	C	11.02	10.56	5.91	2.20	0.65	129	2	MCG +02-60-017
205826.80	-423900.3	LIN	C	11.08	9.69	5.33	1.75	0.65	135	2	ESO 286-19
043400.03	-083444.9	AGN	C	8.74	8.21	3.54	-0.07	0.63	133	2	NGC 1614
131503.51	+243707.8	Q?	C	10.44	10.32	7.05	2.45	0.61	99	2	IC 860
103833.62	-071014.4	G	C	9.49	9.10	4.14	0.80	0.61	146	1	IC 630
181338.76	-574356.9	G	C	11.26	10.84	5.99	2.57	0.60	142	0	IC 4686
225234.71	+244349.4	AGN	C	11.44	10.87	6.06	2.67	0.60	143	2	Mrk 309
151806.13	+424444.8	LIN	C	10.69	10.05	5.60	1.96	0.60	132	2	IRAS F15163+4255-NW
133955.96	-313824.4	AGN	C	8.27	7.00	2.95	-0.73	0.60	130	2	NGC 5253
121539.36	+361935.1	SBG	C	11.13	10.70	6.31	2.59	0.59	128	1	NGC 4228
124930.16	-112403.4	Sy2	C	11.46	10.10	5.90	2.79	0.59	286	1	IRAS 12468-1107
102508.18	+170914.1	IG	C	12.56	12.15	8.06	4.15	0.58	121	0	NGC 3239
231546.75	-590314.5	Sy2	C	10.69	9.67	5.34	1.87	0.57	139	2	ESO 148-2
134442.10	+555313.3	Sy2	C	10.22	9.00	5.36	1.51	0.55	123	2	Mrk 273
121346.00	+024840.3	LIN	C	12.11	11.39	7.02	3.54	0.55	139	2	LEDA 39024
062722.52	-471046.7	IG	C	11.52	11.06	6.66	3.11	0.55	135	3	ESO 255-7
025941.29	+251415.0	G	C	11.89	11.46	6.99	3.49	0.54	138	1	NGC 1156
011607.20	+330521.7	Sy2	C	11.09	9.78	5.70	2.57	0.54	286	0	NGC 449
010426.95	-640712.2	H2G	C	11.23	10.81	6.03	2.78	0.54	150	0	ESO 79-16
003443.48	-000226.6	Sy2	C	11.72	9.98	6.57	3.84	0.54	347	2	2MFGC-403
000820.57	+403755.9	Sy2	C	12.41	12.27	8.58	4.44	0.54	113	3	2MASX J00082041+4037560
021037.63	-154624.2	G	C	10.95	10.49	6.01	2.54	0.54	140	2	NGC 814
005404.02	+730505.7	G	C	9.31	8.75	4.23	0.84	0.54	143	2	MCG+12-02-001
130220.39	-154559.0	GiG	C	9.86	9.43	5.14	1.55	0.53	134	2	MCG-02-33-099
125145.54	+254628.5	IG	C	9.74	9.58	6.24	1.92	0.53	107	2	NGC 4747
134818.91	-505838.8	G	B	11.08	10.65	6.00	2.73	0.52	149	0	2MASX J13481892-5058391
001850.88	-102236.6	EmG	C	10.76	10.29	5.41	2.37	0.52	162	0	MCG-02-01-051
080106.63	-660914.9	G	C	10.20	8.51	5.24	2.17	0.52	338	2	6dFGSg J080106.6-660915
183820.32	-652539.0	Sy2	C	9.37	7.80	4.32	1.21	0.52	322	2	ESO 103-35
043548.45	+021529.6	G	C	11.17	10.03	6.03	2.54	0.52	138	2	UGC 3097
002131.65	-483728.7	IG	C	8.71	8.24	3.89	0.44	0.51	140	2	NGC 92
102751.28	-435414.5	GiG	C	7.48	6.83	2.58	-0.88	0.51	139	2	6dFGSg J102751.3-435414
054323.63	+540044.2	G	B	11.54	11.07	6.52	3.24	0.51	149	2	2MASX J05432362+5400439
064651.13	-645727.7	IG	C	12.10	11.78	7.30	3.90	0.50	142	0	ESO 87-41
105918.14	+243234.6	LIN	C	10.90	10.12	5.63	2.44	0.50	153	0	2XMM J105918.1+243234
130842.02	-242257.8	Sy2	C	11.29	10.22	5.91	2.72	0.50	153	2	PKS 1306-241
033639.05	-205406.8	GiG	C	9.58	7.98	4.69	1.50	0.50	328	2	NGC 1377
002153.60	-791007.8	Sy2	C	10.06	8.39	5.22	2.14	0.49	341	2	2MASX J00215355-7910077
012002.63	+142142.5	LIN	C	10.84	9.67	5.41	2.24	0.49	154	0	MCG+02-04-025
034648.35	+680546.5	GiG	C	6.95	6.61	2.54	-1.12	0.49	131	2	IC 342
022557.05	-244240.8	IG	C	11.80	11.57	7.55	3.82	0.49	127	1	AM 0223-245
233614.11	+020917.9	AGN	C	9.31	9.04	4.73	1.24	0.49	138	2	NGC 7714

¹ *Grade* refers to how well understood an object is (see Section 4.3.) Grade B is reserved for objects with very little presence in the refereed literature, such that we are not convinced the object's true nature has been carefully verified. Grade A is given to objects that are effectively new to science having, at most, been detected in surveys but never examined.

² *Photometry* refers to the source of the photometry used in the table: 0:Profile fit; 1:Aperture-corrected; 2:Calibrated, 3:Elliptical aperture. See Section 5.1

TABLE 9
EXTREME WISE γ SOURCES (GRADES A+B)

NLS #	RA hhmmss.ss	DEC ddmmss.s	SIMBAD type	Grade ¹	W1 mag.	W2 mag.	W3 mag.	W4 mag.	γ	T_{waste} (K) K	Photometry ²	Note
1	224436.12	+372533.6		A	11.27	9.79	6.92	4.44	0.35	381	2	
2	073504.83	-594612.4		A	12.86	12.59	8.03	5.80	0.30	229	0	
3	162721.02	+824538.7	IR	A	13.39	13.18	9.41	6.31	0.27	156	0	IRAS 16329+8252
4	155812.25	-141806.2	IR	B	16.48	15.39	9.13	4.03	0.99	89	0	IRAS 15553-1409
5	031805.43	-663024.0	Cl*	B	12.12	11.69	6.92	3.42	0.61	138	1	[L2004]-n1313-341
6	005342.56	-723920.9	EB*	B	13.17	12.78	8.43	4.77	0.56	131	0	OGLE J005342.56-7239
7	125552.98	-765608.7	HH	B	12.38	10.67	8.14	6.92	0.53	516	3	HH-54H2
8	134818.91	-505838.8	G	B	11.08	10.65	6.00	2.73	0.52	149	0	2MASX J13481892-5058
9	054323.63	+540044.2	G	B	11.54	11.07	6.52	3.24	0.51	149	2	2MASX J05432362+5400
10	214140.73	-454223.0	IR	B	11.57	10.54	7.33	3.28	0.50	115	2	IRAS F21384-4556
11	012933.33	-733344.3	Y*?	B	10.57	9.73	6.57	2.57	0.45	117	2	[GQH2007]-50
12	214035.92	+663525.8	Y*O	B	10.05	8.25	5.58	3.05	0.45	403	1	2MASS J21403852+6635
13	031803.99	-663234.1	WR*	B	13.30	12.93	8.61	5.32	0.45	147	1	[HC2007]-15
14	065558.96	-404912.2	G	B	11.12	10.72	7.34	3.41	0.43	119	2	6dFGSg J065559.0-4049
15	163600.57	+101340.4	G	B	13.09	12.56	8.22	5.09	0.43	156	1	2MASX J16360060+1013
16	061452.97	-062244.4	Y*O	B	8.80	8.31	3.15	1.78	0.42	289	2	IRAS 06124-0621
17	093016.68	+212150.5	G	B	11.75	11.31	6.94	3.86	0.41	159	2	SDSSCGB-51158.1
18	020805.42	-291432.7	G	B	11.64	10.16	6.98	4.19	0.41	346	2	2dFGRSTGS306Z04
19	224458.08	-014600.4	G	B	11.10	10.55	6.18	3.16	0.41	162	2	2MASX J22445816-0146
20	195405.20	+495647.0	G	B	12.57	12.16	7.39	4.81	0.39	195	0	LEDA 200363
21	044738.41	-172601.8	G	B	11.74	11.39	7.38	4.02	0.39	144	2	ESO 552-5
22	113231.06	+742242.0	G	B	11.59	11.30	7.06	3.89	0.39	153	2	2MASX J11323098+7422
23	154813.36	-245309.6	EmG	B	11.29	11.00	6.74	3.59	0.39	155	1	ESO 515-7
24	181603.19	+473705.4	G	B	11.46	11.13	6.79	3.74	0.39	160	2	2MASX J18160312+4737
25	024143.24	+454626.6	G	B	11.71	11.35	7.22	3.99	0.38	150	2	2MASX J02414325+4546
26	045510.80	+053512.6	GiC	B	12.52	12.12	8.00	4.81	0.38	152	2	2MASX J04551070+0535
27	181041.37	+250723.2	G	B	11.88	11.64	7.19	4.23	0.38	166	0	2MASX J18104135+2507
28	061647.61	-090133.6	IR	B	8.64	8.18	3.34	1.60	0.37	280	2	IRAS 06144-0900
29	185222.44	-293620.7	EmG	B	10.77	10.49	6.52	3.18	0.37	144	2	6dFGSg J185222.4-2936
30	134547.40	+700445.9	G	B	11.24	10.87	6.59	3.58	0.37	162	2	2MASX J13454733+7004
31	025559.96	+474819.3	G	B	10.74	10.49	6.39	3.16	0.37	150	2	MCG+08-06-022
32	052134.60	-660547.1	Y*O	B	13.02	12.39	7.88	5.30	0.36	197	1	[GC2009]J052134.67m660
33	083538.40	-011407.1	G	B	11.68	10.65	6.82	4.38	0.36	310	2	2MASX J08353838-0114
34	173429.01	-040541.7	G	B	13.11	12.58	8.20	5.44	0.35	180	0	6dFGSg J173428.9-0405
35	045542.30	-712034.9	Y*?	B	13.52	13.18	8.30	6.55	0.35	273	1	GMP 19
36	195751.88	-322128.2	EmG	B	10.70	10.40	6.28	3.15	0.35	155	2	6dFGSg J195751.9-3221
37	191227.31	-290235.7	EmG	B	11.66	11.33	6.97	4.10	0.35	171	0	ESO 459-7
38	132021.98	-233225.9	EmG	B	11.51	10.67	6.71	3.71	0.35	164	2	2MASX J13202200-2332
39	152309.66	-393448.2	G	B	11.74	11.28	7.13	4.17	0.34	165	0	2MASX J15230967-3934
40	035715.22	-261859.3	G	B	13.96	13.51	9.37	6.39	0.34	164	0	APMBGC 483+082+C0
41	054746.71	-444953.8	IR	B	11.95	11.63	7.49	4.47	0.33	162	2	IRAS 05463-4450
42	064233.41	-645925.4	G	B	13.41	13.12	9.01	5.96	0.33	160	0	AM 0642-645
43	025609.76	-153943.5	G	B	12.60	12.01	8.33	5.04	0.33	147	3	6dFGSg J025609.8-1539
44	042851.45	+693447.1	G	B	11.72	11.32	6.89	4.26	0.33	190	0	2MASX J04285125+6934
45	150253.22	+165508.4	GiG	B	10.85	10.51	6.25	3.40	0.33	172	0	MCG+03m38m076
46	025039.58	+414012.5	IR	B	10.91	10.73	7.24	3.65	0.32	133	1	IRAS 02474+4127
47	102050.93	-171859.4	EmG	B	11.95	11.63	7.38	4.52	0.32	172	0	MCG-03-27-005
48	182552.75	+375241.6	IR	B	12.10	11.91	7.77	4.74	0.32	161	0	IRAS 18241+3750
49	202825.49	-330420.5	G	B	10.33	10.32	7.15	3.29	0.32	121	2	ESO 400-28
50	140330.96	-504643.1	HI	B	13.45	13.38	9.81	6.26	0.32	134	0	HIPASS J1403-50
51	092338.22	-251634.9	EmG	B	11.11	10.86	6.69	3.74	0.32	166	2	6dFGSg J092338.2-2516
52	013506.96	-412611.9	G	B	9.64	9.55	5.76	2.40	0.32	143	2	6dFGSg J013506.9-4126
53	093548.86	-291955.6	EmG	B	11.84	10.62	7.34	5.08	0.32	355	0	ESO 434-13
54	194112.82	+630542.9	G	B	11.76	11.42	7.30	4.37	0.31	167	2	2MASX J19411289+6305
55	105416.74	-394019.3	G	B	11.28	11.07	7.12	3.98	0.31	155	2	ESO 318-23
56	125324.16	-234545.6	EmG	B	12.69	12.43	8.40	5.37	0.31	161	0	6dFGSg J125324.2-2345
57	044016.10	-444525.7	G	B	11.77	11.46	7.38	4.43	0.31	166	2	6dFGSg J044016.1-4445
58	054421.56	-135311.9	G	B	12.02	11.65	7.29	4.70	0.31	192	0	2MASX J05442151-1353
59	174709.21	-643817.6	WR?	B	9.54	9.18	6.11	2.37	0.30	125	2	[CB2009]-A1-C1
60	004250.05	-365243.2	G	B	11.46	11.24	6.87	4.22	0.30	187	0	6dFGSg J004250.1-3652
61	111859.15	-400013.2	G	B	11.45	11.08	6.55	4.42	0.30	248	0	2MASX J11185912-4000
62	051521.42	-262817.1	EmG	B	11.52	11.25	7.34	4.25	0.30	157	2	ESO 486-39
63	040819.05	-611605.7	IG	B	11.11	10.89	6.91	3.87	0.30	160	2	ESO 118-4
64	111932.31	-471015.7	G	B	12.05	11.83	7.94	4.82	0.30	155	2	2MASX J11193186-4710
65	050147.35	-181000.8	IG	B	12.20	11.99	7.57	5.02	0.30	195	0	NGC 1739
66	063226.08	-243208.3	G	B	12.50	12.32	8.13	5.29	0.30	173	0	ESO 490-11
67	070912.66	-440731.7	G	B	12.58	12.40	8.17	5.38	0.29	177	0	ESO 256-16
68	045605.74	+015932.1	G	B	12.17	11.96	7.75	4.97	0.29	177	0	
69	173431.80	+471301.7	G	B	11.75	11.49	7.29	4.54	0.29	179	2	2MASX J17343177+4713
70	222149.97	+395024.0	GiG	B	12.43	12.08	7.63	5.31	0.29	219	1	IRAS 22196+3935
71	105052.15	+010944.2	GiG	B	12.09	11.75	7.36	4.94	0.29	208	0	IC 649S
72	114543.59	-114712.6	EmG	B	11.30	11.00	6.55	4.21	0.29	216	0	6dFGSg J114543.6-1147

TABLE 9 — *Continued*

NLS #	RA hhmmss.ss	DEC ddmmss.s	SIMBAD type	Grade ¹	W1 mag.	W2 mag.	W3 mag.	W4 mag.	γ	T_{waste} (K) K	Photometry ²	Note
73	024506.40	-020727.7	G	B	12.01	11.83	7.93	4.86	0.29	158	3	2MFGC
74	142837.03	-394844.1	IG	B	11.93	11.79	7.60	4.81	0.28	176	2	ESO 32
75	232610.59	-303106.1	EmG	B	11.45	11.14	6.91	4.29	0.28	189	2	6dFGSg J23261
76	161833.99	+132425.9	G	B	13.08	12.63	9.02	5.85	0.28	152	3	2MASX J161833
77	075803.01	-642929.2	G	B	11.89	11.54	7.11	4.93	0.28	238	0	6dFGSg J07580
78	225451.03	+374220.8	IG	B	12.75	12.12	7.96	5.49	0.28	206	1	2MASX J225450
79	064540.95	+433407.5	G	B	11.81	11.61	7.46	4.72	0.27	180	2	2MASX J064540
80	064339.31	-271217.6	GiG	B	10.83	10.64	6.79	3.74	0.27	159	2	6dFGSg J06433
81	202933.28	-441815.2	G	B	12.20	11.97	7.60	5.18	0.27	206	0	2MASX J202933
82	174949.84	-484826.9	PN	B	12.20	12.19	9.16	5.40	0.27	124	0	PN-G343.
83	030445.12	+074739.2	G	B	12.47	12.30	8.34	5.42	0.27	167	0	2MASX J030445
84	055652.46	-052303.8	LSB	B	11.58	11.40	7.78	4.55	0.26	149	2	6dFGSg J05565
85	051646.24	-122059.4	G	B	10.53	10.33	6.44	3.47	0.26	164	1	6dFGSg J05164
86	165033.09	-672039.6	G	B	11.89	11.53	7.28	4.88	0.26	210	0	LEDA 96
87	194605.40	+640850.1	G	B	10.96	10.55	6.97	3.84	0.26	154	2	2MASX J194605
88	120913.87	+265237.4	G	B	12.00	11.82	8.05	5.00	0.26	159	2	LEDA 38
89	235521.97	-563457.1	G	B	13.02	12.71	8.42	6.07	0.26	214	0	6dFGSg J23552
90	054738.65	-103552.8	G	B	12.79	12.50	8.88	5.76	0.25	155	3	6dFGSg J05473
91	140736.99	+160121.6	G	B	12.03	11.68	7.70	4.98	0.25	181	2	2MASX J140736
92	093930.15	+062613.0	G	B	11.98	11.72	7.49	5.04	0.25	203	1	2MASX J093930
93	095814.56	-381356.5		B	12.82	12.68	8.80	5.87	0.25	166	0	

¹ *Grade* refers to how well understood an object is (see Section 4.3.) Grade B is reserved for objects with very little presence in the refereed literature, such that we are not convinced the object's true nature has been carefully verified. Grade A is given to objects that are effectively new to science having, at most, been detected in surveys but never examined.

² *Photometry* refers to the source of the photometry used in the table: 0:Profile fit; 1:Aperture-corrected; 2:Calibrated, 3:Elliptical aperture. See Section 5.1